

1 **Observation of Isoprene Hydroxynitrates in the Southeastern**
2 **United States and Implications for the Fate of NO_x**

3
4 **F. Xiong¹, K. M. McAvey¹, K. A. Pratt^{1,3}, C. J. Groff¹, M. A.**
5 **Hostetler¹, M. A. Lipton¹, T. K. Starn⁴, J. V. Seeley⁵, S. B. Bertman⁶,**
6 **A. P. Teng⁷, J. D. Crounse⁸, T. B. Nguyen⁸, P. O. Wennberg^{7,8}, P. K.**
7 **Misztal⁹, A. H. Goldstein^{9,10}, A. B. Guenther¹¹, A. R. Koss^{12,13}, K. F.**
8 **Olson⁹, J. A. de Gouw^{12,13}, K. Baumann¹⁴, E. S. Edgerton¹⁴, P. A.**
9 **Feiner¹⁵, L. Zhang¹⁵, D. O. Miller¹⁵, W. H. Brune¹⁵ and P. B.**
10 **Shepson^{1,2}**

11 [1] Department of Chemistry, Purdue University, West Lafayette, IN

12 [2] Department of Earth, Atmospheric and Planetary Sciences, Purdue University, West
13 Lafayette, IN

14 [3] Department of Chemistry, University of Michigan, Ann Arbor, MI

15 [4] Department of Chemistry, West Chester University of Pennsylvania, West Chester,
16 PA

17 [5] Department of Chemistry, Oakland University, Rochester, MI

18 [6] Department of Chemistry, Western Michigan University, Kalamazoo, MI

19 [7] Division of Engineering and Applied Science, California Institute of Technology,
20 Pasadena, CA

21 [8] Division of Geophysical and Planetary Sciences, California Institute of Technology,
22 Pasadena, CA

23 [9] Department of Environmental Science, Policy, & Management, University of
24 California at Berkeley, Berkeley, CA

25 [10] Department of Civil and Environmental Engineering, University of California at
26 Berkeley, Berkeley, CA

27 [11] Atmospheric Sciences and Global Change Division, Pacific Northwest National
28 Laboratory, Richland, WA

29 [12] Cooperative Institute for Research in Environmental Sciences, Boulder, CO

30 [13] NOAA Earth System Research Laboratory, Boulder, CO

31 [14] Atmospheric Research & Analysis, Inc., Cary, NC

32 [15] Department of Meteorology, Pennsylvania State University, University Park, PA

33 Correspondence to: P. B. Shepson (pshepson@purdue.edu)

34

35 **Abstract**

36 Isoprene hydroxynitrates (IN) are tracers of the photochemical oxidation of isoprene in
37 high NO_x environments. Production and loss of IN have a significant influence on the
38 NO_x cycle and tropospheric O₃ chemistry. To better understand IN chemistry, a series of
39 photochemical reaction chamber experiments was conducted to determine the IN yield
40 from isoprene photooxidation at high NO concentrations (>100 ppt). By combining
41 experimental data and calculated isomer distributions, a total IN yield of 9(+4/-3)% was
42 derived. The result was applied in a zero-dimensional model to simulate production and
43 loss of ambient IN observed in a temperate forest atmosphere, during the Southern
44 Oxidant and Aerosol Study (SOAS) field campaign, from May 27 to July 11, 2013. The 9%
45 yield was consistent with the observed IN/(MVK+MACR) ratios observed during SOAS.
46 By comparing field observations with model simulations, we identified NO as the
47 limiting factor for ambient IN production during SOAS, but vertical mixing at dawn
48 might also contribute (~27%) to IN dynamics. A close examination of isoprene's
49 oxidation products indicates that its oxidation transitioned from a high-NO dominant
50 chemical regime in the morning into a low-NO dominant regime in the afternoon. A
51 significant amount of IN produced in the morning high NO regime could be oxidized in
52 the low NO regime, and a possible reaction scheme was proposed.

53 1 Introduction

54 Isoprene (C₅H₈) accounts for approximately half of the global non-methane biogenic
55 volatile organic compound (BVOC) emissions (Guenther et al., 2006) and has a
56 significant influence on the budgets of OH, O₃ and NO_x (Horowitz et al., 2007). Isoprene
57 oxidation by OH in the presence of NO_x can lead to the formation of isoprene
58 hydroxynitrates (IN), as described in Reactions (R1) and (R2). The chain-terminating
59 Reaction (R2a) removes peroxy radicals (RO₂) and NO from the atmosphere and
60 decreases tropospheric O₃ production (Carter and Atkinson, 1996). IN serves as a
61 temporary NO_x reservoir, and the transport and photo-oxidative decomposition of these
62 compounds can further modulate NO_x and O₃ concentrations (Horowitz et al., 2007;
63 Paulot et al., 2012; Xie et al., 2013). Gas-phase organic nitrates can also partition into the
64 particle phase and undergo hydrolysis, contributing to the growth of secondary organic
65 aerosols (SOA) (Jacobs et al., 2014; Rindelaub et al., 2015).



69 The initial OH addition (followed by O₂) to isoprene (Reaction R1) produces eight
70 isomeric RO₂ radicals. Reaction of these RO₂ radicals with NO proceeds primarily via
71 two reaction pathways (Reaction R2a and b). Laboratory studies suggest that the nitrate
72 formation channel (Reaction R2a) is minor compared to the alkoxy radical (RO)
73 formation channel (Reaction R2b), with reported total IN yields ranging from 4% to 14%
74 (Chen et al., 1998; Patchen et al., 2007; Lockwood et al., 2010; Paulot et al., 2009;
75 Sprengnether et al., 2002; Tuazon and Atkinson, 1990). Reaction (R2a) leads to the
76 formation of eight IN isomers, including four β-IN isomers and four δ-IN isomers (Table
77 1). The wide range of reported IN yields has led to uncertainty in quantifying isoprene's
78 influence on the NO_x cycle and O₃ enhancement (Xie et al., 2013; Horowitz et al., 2007;
79 Paulot et al., 2012). Isoprene hydroxynitrates can also be produced at night through NO₃-
80 initiated isoprene oxidation with a yield around 20%, adding to a total organic nitrate
81 yield of 65-70% (Rollins et al., 2009; Perring et al., 2009; Kwan et al., 2012). The major
82 daytime IN sink is reaction with OH, which leads to a lifetime of 2.5 to 6.5 hours,

83 according to a recent kinetics study (Lee et al., 2014b). At night, IN is more susceptible
84 to loss from ozonolysis, and potentially NO₃ oxidation when the NO_x concentration is
85 high (Xie et al., 2013). IN have been observed in the ambient environment, primarily in
86 forested areas under the influence of anthropogenic NO_x plumes (Grossenbacher et al.,
87 2001; Giacomelli et al., 2005; Grossenbacher et al., 2004; Beaver et al., 2012; Lee et al.,
88 2014a). During the BEARPEX 2009 study conducted in the Sierra Nevada Mountains of
89 California, IN constituted 38% of the total organic nitrates (Beaver et al., 2012).

90 Methods to quantify organic nitrates include infrared spectroscopy (IR), thermal
91 dissociation-laser induced fluorescence (TD-LIF) spectroscopy, chemiluminescence, gas
92 chromatography (GC)-based separation and detection techniques, and mass spectrometry
93 (MS) (Rollins et al., 2010; Tuazon and Atkinson, 1990; Sprengnether et al., 2002; Day et
94 al., 2002; O'Brien et al., 1995; Beaver et al., 2012; Lee et al., 2014a; Lockwood et al.,
95 2010; Paulot et al., 2009; Giacomelli et al., 2005; Grossenbacher et al., 2004; Patchen et
96 al., 2007; Hartsell et al., 1994; Kwan et al., 2012; Teng et al., 2015). IR, TD-LIF, and
97 chemiluminescence can only measure total organic nitrates because they respond solely
98 to the nitrooxy functional group (Day et al., 2002; Rollins et al., 2010; Tuazon and
99 Atkinson, 1990; Sprengnether et al., 2002; O'Brien et al., 1995; Hartsell et al., 1994).
100 GC- and MS-based methods can speciate organic nitrates and have been employed
101 previously to quantify IN in both laboratory and field studies (Lockwood et al., 2010;
102 Patchen et al., 2007; Giacomelli et al., 2005; Paulot et al., 2009; Lee et al., 2014a;
103 Grossenbacher et al., 2004; Beaver et al., 2012; Kwan et al., 2012). For MS-based
104 techniques, the fragile O-NO₂ bond in organic nitrates often fragments during ionization
105 (Perring et al., 2009), so soft-ionization methods with reagent ion such as H⁺(H₂O)₄,
106 CF₃O⁺, and I⁺ are necessary to detect the molecular ion for organic nitrates (Patchen et al.,
107 2007; Beaver et al., 2012; Lee et al., 2014a; Crounse et al., 2006).

108 Here we present a comprehensive laboratory and field study of the formation of IN from
109 isoprene reaction with OH. In the summer of 2013, we quantified ambient IN in rural
110 Alabama for 6 weeks during the Southern Oxidant and Aerosol Studies (SOAS,
111 <http://soas2013.rutgers.edu/>). In parallel with the field study, laboratory experiments were
112 conducted to determine the yield of IN from isoprene oxidation. For laboratory
113 experiments, we synthesized authentic standards for the quantification of IN, using

114 multiple calibration techniques. The IN yield obtained from lab experiments was applied
115 in a zero-dimensional model to simulate IN production and loss in the atmosphere, which
116 was then compared with the measurements from SOAS, to examine our understanding of
117 atmospheric IN chemistry.

118 **2 Experiment**

119 **2.1 CIMS IN calibration**

120 A chemical ionization mass spectrometer (CIMS) was used to measure IN concentrations
121 during the chamber experiments and the SOAS field study. The instrument is similar to
122 the one described by Liao et al. (2011), which uses $I(H_2O)_n^-$ to form iodide clusters with
123 the analyte compounds.

124 Two authentic standards, 4,3-IN and 1,4-IN (a mixture of *trans*- and *cis*-1,4-IN), were
125 synthesized to determine the sensitivity of CIMS toward IN isomers. 1,4-IN was prepared
126 using the nitrification method described by Lee et al. (2014b), and the sample was used
127 after flash column chromatography without further purification to separate the *trans* and
128 *cis* isomers. 4,3-IN was prepared by nitrification of (1-methylethenyl)oxirane, and the
129 epoxide was synthesized following Harwood et al. (1990).

130 The IN gas-phase sample for CIMS calibration was prepared by evaporating an IN/C₂Cl₄
131 standard solution of known volume into 50 L of clean air. The IN concentration in the
132 standard solution was determined with NMR and FTIR, and the results from the two
133 methods were consistent within 15%. Multiple CIMS calibrations for 4,3-IN were
134 performed, and the results did not deviate more than 15% after 1.5 years (Supplement
135 Sect. 1). The average sensitivity of 4,3-IN normalized to the reagent ion signal was
136 $2.3(\pm 0.3) \times 10^{-3} \text{ ppt}^{-1}$.

137 The 1,4-IN calibration was conducted following the same procedures. Since the 1,4-IN
138 standard contained a mixture of *trans*- and *cis*-1,4-IN, the measured sensitivity was a
139 weighted average of both isomers. The relative abundance of the *trans*- and *cis*-1,4-IN
140 isomers was obtained from NMR, and their individual sensitivities were estimated using
141 a least-squares method (Supplement Sect. 2). The CIMS sensitivity was $3(\pm 2) \times 10^{-4} \text{ ppt}^{-1}$
142 for *trans*-1,4-IN and $1.3(\pm 0.3) \times 10^{-3} \text{ ppt}^{-1}$ for *cis*-4,1-IN.

143 As we were unable to synthesize the 1,2-IN standard in the condensed phase, a relative
144 method was used, where the CIMS was interfaced with a GC equipped with an electron
145 capture detector (ECD, Figure 1) to determine the CIMS sensitivity of 1,2-IN relative to
146 4,3-IN. A mixture of the eight IN isomers was generated by irradiation of a mixture of
147 isoprene, isopropyl nitrite, and NO. The IN mixture was cryo-focused at the head of a 4
148 m Rtx-1701 column that separated the IN isomers, and the effluent was split into two
149 fused-silica deactivated transfer columns, directed simultaneously to the CIMS and the
150 ECD.

151 As the CIMS was operated with water addition to the sample gas before ionization, the
152 GC-ECD/CIMS setup enabled direct observation of the influence of water vapor to the
153 sensitivity of the two dominant IN isomers. Figure 2 shows the GC-ECD/CIMS
154 chromatograms with and without water added to the CIMS. The change in retention time
155 was the result of change in initial oven temperature setting, which had little influence on
156 the elution temperature of IN. 1,2-IN and 4,3-IN were the dominant IN isomers and 1,2-
157 IN eluted before 4,3-IN, according to a recent study using the same stationary phase
158 (Nguyen et al., 2014b). 1,2-IN and 4,3-IN are expected to have the same ECD sensitivity,
159 because the ECD has similar response to all mono-nitrates and the hydroxyl group in
160 hydroxynitrate has no influence on ECD sensitivity (Hao et al., 1994). Therefore, the
161 CIMS sensitivity of 1,2-IN relative to 4,3-IN was calculated as the ratio of the CIMS
162 signal intensity to the corresponding ECD signal intensity, for the pair of isomers. The
163 calculated relative CIMS sensitivity was $0.37(\pm 0.06)$ with water and $0.95(\pm 0.06)$ without
164 water added, determined as the average of three trials for each setup. The result indicated
165 that water addition to the sample air lowered the CIMS sensitivity to the 1,2-IN isomer.
166 The small abundance of the other isomers makes it difficult to obtain reliable
167 quantification through this method. Therefore, the sensitivities for cis- and trans-1,4-IN
168 were obtained with a synthesized standard.

169 The CIMS sensitivities toward alkyl alcohols and alkyl nitrates are both around 5 orders
170 of magnitude smaller than its sensitivity toward the isoprene hydroxynitrates. Hence, it is
171 the combination of the OH group and the NO₃ group, as well as their relative positions
172 that has the dominant influence on the CIMS sensitivity, which will affect how the
173 molecule binds with the iodide ion, while the structure of the carbon backbone would

174 have little effect. For the IN isomers, the relative positions of the OH group and the
175 nitrate group are α,β position, $trans-\alpha,\delta$ position and $cis-\alpha,\delta$ position. We assume the
176 same sensitivity can be applied to isomers within each structural group, namely β -
177 isomers, *trans*- δ isomers and *cis*- δ isomers. This assumption is consistent with our
178 observation of identical sensitivity for 1,2-IN and 4,3-IN isomers when water is not
179 added to the CIMS. For the case with water addition to CIMS, the smaller sensitivity of
180 the 1,2-IN was caused by the smaller amount of 1,2-IN available for detection, as 1,2-IN
181 is lost inside the instrument, rather than from a fundamental difference in the ionization
182 efficiency of 1,2-IN. Primary nitrates (δ -IN, 3,4-IN, and 2,1-IN) and secondary nitrates
183 (4,3-IN) are not as likely to be affected by water (Hu et al., 2011). As a result, *cis*-1,4-IN
184 was used as a surrogate for *cis*-4,1-IN, and *trans*-1,4-IN was used a surrogate for *trans*-
185 4,1-IN. For the β -IN isomers, 1,2-IN had to be considered separately due to its loss inside
186 the instrument, but 4,3-IN was used as a surrogate for 3,4- and 2,1-IN isomers. Our
187 assignment of CIMS sensitivities for IN isomers is consistent with reports from Lee et al.
188 (2014a). Given the significant difference in sensitivity for different IN isomers, the CIMS
189 IN data have to be interpreted with the knowledge of relative IN isomer distribution,
190 which depends on both IN production and loss. Since the IN isomer distribution was not
191 measured in either the laboratory or the field studies, model simulation was used to
192 estimate the relative abundance of IN isomers. The distribution of IN isomers during the
193 chamber experiments was estimated using an iterative method (Supplement Sect. 3.1).
194 For IN measurement during SOAS, a diurnal average of the changing IN isomer
195 distribution (Figure S9) was estimated and applied to calibrate IN data for each individual
196 day. The isomer-weighted IN sensitivity changed by less than 20% throughout the day
197 (Supplement Sect. 3.2).

198 **2.2 Isoprene chamber experiments**

199 Seven experiments were conducted in the 5500 L Purdue photochemical reaction
200 chamber (Chen et al., 1998) to determine the yield of IN from OH-initiated isoprene
201 oxidation in the presence of NO_x . OH was generated from the photolysis of isopropyl
202 nitrite. The starting conditions for the experiments are listed in Table 2. Each experiment

203 was initiated by switching on the UV lamps and was considered complete when half of
204 the isoprene was consumed or the NO concentration dropped to around 5 ppb.

205 The IN concentration was measured continuously during each experiment with the CIMS.
206 Chamber air was sampled through a 5.2 m long inlet, made of 0.8 cm ID heated (constant
207 50 °C) FEP Teflon tubing. A total flow of 5 liters per minute (lpm) was pulled through
208 the inlet into a custom-built three-way valve system (Liao et al., 2011), where 2 lpm was
209 sub-sampled into the CIMS through a 0.51 mm orifice. Water vapor was added
210 downstream of the orifice to humidify the sample air to reduce the influence that
211 variations in ambient RH and temperature have on the distribution of $I(\text{H}_2\text{O})_n^-$ clusters.
212 Laboratory tests showed that with constant H_2O addition, the CIMS sensitivity is not
213 dependent on ambient air humidity (Supplement Sect. 6). The fractional loss inside the 50
214 °C sampling inlet was measured to be 5 % for a mixture of the eight IN isomers.

215 Isoprene and its oxidation products, methyl vinyl ketone (MVK) and methacrolein
216 (MACR), were quantified with a proton-transfer reaction linear ion trap mass
217 spectrometer (PTR-LIT MS), with measurement precision of 3 ppb and accuracy of $\pm 17\%$
218 (Mielke et al., 2010). MVK and MACR were observed as the same nominal mass without
219 further differentiation for relative isomeric abundance. The NO concentration was
220 measured through chemiluminescence using the total reactive nitrogen instrument
221 (TRENI) (Lockwood et al., 2010), and the addition of isopropyl nitrite did not cause any
222 interference signal for TRENI during the chamber experiments.

223 One wall loss experiment was conducted by keeping the IN isomers produced from
224 isoprene oxidation in the dark chamber and sampling the chamber air with CIMS
225 periodically for four hours. No significant IN loss was observed, so no wall loss
226 correction was applied for IN measurement.

227 **2.3 CIMS SOAS measurement**

228 During SOAS, the CIMS was used to measure ambient IN concentrations continuously
229 from May 26st to July 11th, 2013 at the Centerville (CTR) site (32.90° N, 87.25° W). The
230 CTR site is located about 50 miles south of Birmingham and Tuscaloosa near the
231 Talladega National Forest, a region abundant with pine and oak trees. The CIMS was

232 operated under the same conditions as those during the chamber experiments, in terms of
233 voltage setting, gas flow and sample humidification. Air was sampled from 5.3 m above
234 the ground, with the same inlet (heated to constant 50 °C) and valve system that were
235 used for chamber experiments. The CIMS three-way valve system was used to allow
236 automated background measurement and in-situ Br₂ calibration to monitor instrument
237 stability. The background was determined by passing ambient air through nylon wool
238 coated with sodium bicarbonate for 2 minutes every 15 minutes (Crouse et al., 2006).
239 Laboratory tests suggested that the scrubber removes isoprene-derived organic nitrates,
240 including hydroxynitrates, carbonyl nitrates and hydroxyperoxy nitrates, and acids such
241 as nitric acid and formic acid. Br₂ calibration was performed hourly by adding a 30 sccm
242 Br₂/N₂ flow from a Br₂ permeation device to the ambient air being sampled into the
243 CIMS for 2 min. The CIMS sensitivity to IN was calibrated relative to the Br₂ sensitivity,
244 which were both normalized to the reagent ion signal I(H₂¹⁸O)⁻. The Br₂ output rate from
245 the permeation device was determined daily with the optical absorption method following
246 Liao et al. (2011). The averaged Br₂ output of the permeation source throughout the
247 campaign was 60(±8) ng/min, which was 1.8(±0.2) ppb when diluted with ambient air.

248 **2.4 0D Model for IN Data Interpretation**

249 A zero-dimensional (0D) model based on the Master Chemical Mechanism (MCMv3.2)
250 (Jenkin et al., 1997; Saunders et al., 2003) was used to investigate the production and loss
251 of IN in the chamber and in the SOAS field study. The mechanism was updated for
252 recent experimental and theoretical studies of isoprene chemistry, including the
253 interconversion of isomeric isoprene RO₂ radicals (LIM1) (Peeters et al., 2014), IN
254 reaction rate constants for OH and O₃ (Lee et al., 2014b), IEPOX reaction rate constants
255 for OH (Bates et al., 2014) and the branching ratio for NO₃ addition to isoprene (Fan and
256 Zhang, 2004).

257 For the IN observations during SOAS, our analysis is focused on the production and loss
258 of IN. Therefore, the 0D model for the SOAS data analysis was constrained to the
259 observed concentrations of the major species involved in the IN chemistry, including
260 isoprene, HO_x, O₃, NO_x, α-pinene, β-pinene and limonene. The NO₂ photolysis frequency
261 in the 0D model (J_{NO_2}) was calculated using the Tropospheric Ultraviolet & Visible

262 (TUV) Radiation Model (Madronich and Flocke, 1998) for clear sky conditions with 300
263 DU ozone, and the model input was scaled relative to observed radiation. The photolysis
264 frequencies for all the other species were scaled relative to J_{NO_2} at zero-degree solar
265 zenith angle.

266 Because the 0D model does not take into account the changes in IN concentration as IN
267 was transported to and out of the measurement site both vertically and horizontally, the
268 ratio of total IN concentration to the sum of methyl vinyl ketone (MVK) and
269 methacrolein (MACR) was used to compare the model results with observations. Major
270 sources of MVK and MACR include isoprene ozonolysis (Grosjean et al., 1993) and OH-
271 initiated isoprene oxidation (Liu et al., 2013). As IN, MVK and MACR are produced
272 simultaneously in the isoprene photochemical oxidation process, the ratio
273 $[\text{IN}]/([\text{MVK}]+[\text{MACR}])$ may reduce the influence of dilution caused by vertical mixing
274 and changing boundary layer height, making results from the 0D model comparable to
275 ambient observations. Besides chemical loss to reaction with OH, O_3 and NO_3 , the model
276 also included loss for dry deposition for IN, MVK and MACR, with averaged daytime
277 deposition velocities of 1.5cm/s, 0.7cm/s and 0.4cm/s (Nguyen et al., 2015; Zhang et al.,
278 2002).

279 Isoprene data from the PTR-ToF-MS measurement (Misztal et al., In preparation) were
280 used to constrain the model and its MVK+MACR data were used for model-observation
281 comparison for most days. The MVK and MACR data from the GC-MS measurement
282 (Gilman et al., 2010) were used when knowledge of the relative abundance of MVK and
283 MACR was required to calculate their initial concentrations in the model and when PTR-
284 ToF-MS data were unavailable. The PTR-ToF-MS data were used primarily because of
285 its higher time resolution. Model constraints on α -pinene, β -pinene and limonene
286 concentrations were based on measurements from GC-MS, and 2D-GC when GC-MS
287 data were unavailable.

288 **3 Results**

289 **3.1 IN yield from chamber experiments**

290 The IN yield was calculated from the production of IN relative to the loss of isoprene,
291 using data obtained in the photochemical reaction chamber experiments. The isomer-
292 weighted IN sensitivity is expected to change during each experiment, as IN isomers are
293 lost to OH consumption with different reaction rate constants. To account for the change
294 in IN isomer distribution during each experiment, an iterative method was applied to
295 derive a self-consistent set of total IN yield, IN isomeric distribution and isomer-
296 weighted IN sensitivity (Supplement 3.1). IN loss by OH oxidation was corrected
297 (Atkinson et al., 1982) with an isomer-weighted rate constant to account for the
298 difference in OH reactivity for different isomers (Lee et al., 2014b). The correction factor
299 was around 25% by the end of each experiment. Figure 3 shows the results from the IN
300 yield chamber experiments. The average IN yield was 9%, based on the slope of ΔIN vs.
301 $(-\Delta\text{isoprene})$. We note that the yield has no apparent [NO] dependence with [NO] varying
302 in the range from 125 ppb to 2400 ppb.

303 The relative uncertainty for isoprene concentrations is 17% based on instrument
304 calibration. The uncertainty for IN concentrations is caused by both the uncertainty in the
305 CIMS sensitivity for each IN isomer and the uncertainty in the relative abundance of the
306 IN isomers. Through a sensitivity test on the RO_2 interconversion rate constants of the
307 LIM1 mechanism (Supplement Sect. 5), the IN measurement uncertainty was estimated
308 to be +23%/-20%. The fractional loss for the CIMS inlet was 4(\pm 6)%, making the IN
309 measurement uncertainty to be +24%/-20%. The uncertainty in the reported rate constants
310 for IN oxidation could cause 20 % error when IN data was corrected for OH consumption.
311 Therefore, the overall relative uncertainty in our IN yield is +36%/-33% and we report
312 our total IN yield to be 9(+4/-3)% to encompass all the measurement uncertainties. This
313 result lies in the middle of the 4-14% range of IN yields determined from previous
314 experiments (Chen et al., 1998; Patchen et al., 2007; Lockwood et al., 2010; Paulot et al.,
315 2009; Sprengnether et al., 2002; Tuazon and Atkinson, 1990). Previous IN studies
316 conducted in our group using GC methods consistently resulted in lower IN yields (Chen
317 et al., 1998; Lockwood et al., 2010). We partially attribute the discrepancy of our

318 previous and current work to the possible loss of the 1,2-IN isomer in the GC column and
319 metal sample injection system. This work employed MS to quantify IN during the
320 chamber experiments to circumvent these problems. The current yield result will be
321 applied in the 0D model to simulate IN concentrations during SOAS. The model-
322 measurement agreement offers a metric to evaluate the validity of the laboratory-derived
323 IN yield

324 **3.2 Observation of IN during SOAS**

325 Figure 4 shows the temporal profile of total IN mixing ratio observed during the SOAS
326 field study with an averaging 10-minute time resolution. In general, fast IN production
327 was observed after sunrise. On average, the concentration rose to peak around 70 ppt at
328 10:00 AM (Figure 5) and then decreased to a minimum around 10 ppt by 6:00 AM the
329 next day, as a result of vertical mixing, boundary layer expansion, dry deposition and
330 further oxidation. IN concentrations were significantly lower from Jul 4 to Jul 8, due to
331 wet deposition and less photochemical reactivity caused by continuous rain events.

332 In contrast to the IN average diurnal profile (Figure 5), the diurnal profiles for isoprene,
333 OH, and NO_x and MVK+MACR, each peaked at different times of the day (Figure 6).
334 While IN and MVK + MACR are products of the parallel RO₂ + NO Reactions (R2a and
335 b), the diurnal MVK + MACR concentrations are more consistent with the temporal
336 profiles of isoprene, OH and O₃ with peak concentration around 1:00 PM when radiation
337 was strong. The decrease in IN, and continued increase of MVK and MACR around
338 10:00 AM can be attributed to the competition among the four RO₂ loss channels (R2,
339 R3, R4, and R5).



343 The fraction of RO₂ loss to NO reaction is defined as γ , which is calculated with the
344 following equation.

$$345 \gamma = \frac{k_{\text{RO}_2+\text{NO}}[\text{NO}]}{k_{\text{RO}_2+\text{NO}}[\text{NO}] + k_{\text{RO}_2+\text{HO}_2}[\text{HO}_2] + k_{\text{RO}_2+\text{RO}_2}[\text{RO}_2] + k_{\text{isomerize}}} \quad (1)$$

346 Isoprene RO₂ loss to permutation reactions R4 was calculated assuming [RO₂]=[HO₂],
 347 and the rate constant $1.6 \times 10^{-13} \text{ cm}^3 \text{ molecule}^{-1} \text{ s}^{-1}$ was used (Jenkin et al., 1997). Isoprene
 348 RO₂ loss rates for reaction with NO and HO₂ (R2 and R3) were calculated based on
 349 observed NO and HO₂ concentrations, using rate constants $k_{\text{RO}_2+\text{NO}} = 9 \times 10^{-12} \text{ cm}^3$
 350 $\text{molecule}^{-1} \text{ s}^{-1}$ and $k_{\text{RO}_2+\text{HO}_2} = 1.61 \times 10^{-11} \text{ cm}^3 \text{ molecule}^{-1} \text{ s}^{-1}$ (Saunders et al., 2003; Stevens
 351 et al., 1999). The sum of the first-order RO₂ loss rate for reaction with NO, HO₂ and RO₂
 352 was 0.01-0.07 s⁻¹ (Figure 7a). Therefore, contribution from 1,5-H shift for β-RO₂ was
 353 negligible, due to the small isomerization rate constant (Peeters et al., 2014). However,
 354 for isoprene *cis*-δ-RO₂, the 1,6-H shift rate constant is on the order of 0.1-1s⁻¹ (Peeters et
 355 al., 2009; Crouse et al., 2011; Peeters et al., 2014). This fast isomerization depletes *cis*-
 356 δ-RO₂ radicals rapidly to form closed-shell products, e.g. hydroperoxy aldehyde
 357 (HPALD), and makes the relative abundance of *cis*-δ-RO₂ radicals very small (~1%,
 358 Supplement Sect. 4). For this reason, $k_{\text{isomerize}}$ was omitted from the calculation of γ , but
 359 the yield of total RO₂ was incorporated when estimating the production rate of total IN, to
 360 account for rapid loss of *cis*-δ-RO₂ to 1,6-H shift. In addition, the fast 1,6-H
 361 isomerization for *cis*-δ-RO₂ decreased the production rates of δ-IN among the IN
 362 isomers. With this smaller production rates and their faster loss rates to OH and O₃ (Lee
 363 et al., 2014b), the relative abundance of δ-IN during this field study was much smaller
 364 than what have been observed in laboratory studies (Lockwood et al., 2010; Paulot et al.,
 365 2009).

366 The calculated diurnal average of the γ value is shown in Figure 7b. For RO₂ radicals that
 367 were lost to reaction with NO or HO₂, the RO₂+NO reaction was the sole contributor in
 368 the early morning, but it was surpassed by RO₂+HO₂ reaction before noon, as the NO
 369 concentration decreased steadily throughout the day. The IN production rate was
 370 calculated with the following equation.

$$371 \quad P_{\text{IN}} = k_{\text{ISOP}+\text{OH}}[\text{OH}][\text{ISOP}] \cdot \Phi \cdot \gamma \cdot \alpha \quad (2)$$

372 α is the branching ratio ($=k_{2a}/(k_{2a} + k_{2b})$) for isoprene RO₂ + NO reaction for nitrate
 373 formation. Φ is the yield of total RO₂ from OH addition to isoprene that are available to
 374 react with NO, HO₂ and RO₂, with an RO₂ lifetime in the range of 10~20s. The
 375 calculated Φ is 0.83 (Supplement Sect. 4), with contribution from β-RO₂ being 0.81, *cis*-

376 δ -RO₂ being 0.01 and *trans*- δ -RO₂ being 0.02, and the remaining 17% products from
377 isoprene OH oxidation are closed-shell species such as HPALD.

378 γ value peaked around 6:00 AM to 8:00 AM when the isoprene and OH concentrations
379 were relatively low. During this period, the IN production rate was limited by the
380 availability of RO₂. In the afternoon, when isoprene RO₂ was more abundant with higher
381 isoprene and OH concentrations, the IN production rate was limited by the availability of
382 NO, and decreased with the declining γ value (Fig. 7b) The declining γ value could lead
383 to IN loss from OH oxidation to exceed IN production, making IN peak around the time
384 when HO₂ reaction became the major RO₂ loss channel ($\gamma < 0.5$). In this relatively clean
385 environment, MVK and MACR production continued through isoprene ozonolysis
386 (Grosjean et al., 1993) and OH oxidation in the low NO regime (Liu et al., 2013). The
387 MVK+MACR production rate was calculated using the following equation.

$$\begin{aligned} 388 \quad P_{\text{MVK+MACR}} &= k_{\text{ISOP+OH}}[\text{OH}][\text{ISOP}] \cdot \Phi_{\beta} \cdot \gamma \cdot (1-\alpha) \\ 389 &+ k_{\text{ISOP+OH}}[\text{OH}][\text{ISOP}] \cdot \Phi \cdot (1-\gamma) \cdot 0.06 \\ 390 &+ k_{\text{ISOP+O}_3}[\text{O}_3][\text{ISOP}] \cdot 0.61 \end{aligned} \quad (3)$$

391 Φ_{β} denotes the yield of isoprene β -RO₂, the precursors for MVK+MACR, and the
392 calculated Φ_{β} was 0.81 (Supplement Sect. 4). The term $k_{\text{ISOP+OH}}[\text{OH}][\text{ISOP}] \cdot \Phi_{\beta} \cdot \gamma \cdot (1-\alpha)$ is
393 the production rate of MVK+MACR with the isoprene β -RO₂ undergoing the RO₂+NO
394 reaction pathway. The term $k_{\text{ISOP+OH}}[\text{OH}][\text{ISOP}] \cdot \Phi \cdot (1-\gamma) \cdot 0.06$ is the production rate of
395 MVK+MACR when the isoprene RO₂ proceeds via HO₂+RO₂ reaction pathways to form
396 MVK+MACR with an overall yield of 6% (Liu et al., 2013). The term
397 $k_{\text{ISOP+O}_3}[\text{O}_3][\text{ISOP}] \cdot 0.61$ is the production rate of MVK+MACR from isoprene
398 ozonolysis, with a total yield of 61% (Grosjean et al., 1993).

399 As shown in Figure 7b, the production rates of IN and MVK+MACR both plateaued
400 around 10:00 AM. For MVK+MACR, the decrease was later compensated with
401 production from the HO₂ and O₃ pathway, and the production rate peaked around 2:00
402 PM when radiation was strong. For IN, however, its production rate did not increase with
403 radiation due the limited availability of NO (small γ value). Therefore, the change in the
404 relative importance of the two RO₂ sinks, RO₂+NO and RO₂+HO₂, is likely one of the

405 reasons that the IN concentration peaked earlier than the MVK+MACR concentration
406 during SOAS.

407 The early morning increase in IN concentration could imply significant contribution from
408 downward mixing of accumulated IN in the residual layer (RL), as the inversion is
409 broken up after dawn (Hastie et al., 1993). When the earth surface cools in the evening,
410 the remnants of the upper daytime boundary layer are isolated from the lower region near
411 the ground, and the RL forms. The RL contains the same amount of isoprene, IN, and
412 NO_x as is found near the ground around sunset, thus serving as an IN reservoir at night
413 (Neu et al., 1994). While IN in the nighttime boundary layer (NBL) is slowly lost to dry
414 deposition, IN in the RL, which is isolated from the ground, is better preserved. In
415 addition, IN production from reaction of isoprene with NO_3 may also contribute to RL
416 IN, but this process is not as important in the NBL, because the $\text{NO}_3 + \text{NO}$ reaction near
417 the ground makes the NO_3 concentrations smaller (Stutz, 2004). As a result, the IN
418 concentration in the RL is expected to be higher than that in the NBL before dawn.
419 Perhaps more importantly, the relative volume fraction of NBL vs. RL is small (~ 0.1),
420 and thus surface level nighttime chemistry cannot contribute significantly to the surface
421 IN increase at ~ 10 am. During sunrise, IN in the RL can mix downward, which in
422 combination with photochemical IN production leads to an increase in IN near the
423 ground. The relative importance of these two processes will be assessed with our 0D
424 model in the following section.

425 It is worth mentioning that the nighttime ground-level IN production from $\text{NO}_3 +$
426 isoprene can afford a different IN isomer distribution, which can influence the isomer-
427 weighted IN sensitivity. However, the 0D model simulation of IN isomer distribution has
428 included IN formation from the $\text{NO}_3 +$ isoprene pathway. Therefore, our interpretation of
429 the SOAS IN measurement data has considered the changing IN isomer distribution from
430 both the OH- and the NO_3 -initiated IN production near ground.

431 **3.3 0D model for IN photochemistry during SOAS**

432 Due to limited availability of overlapping data for model input from multiple instruments,
433 ambient data for the following 12 days were used: Jun 14, Jun 16, Jun 22-Jun 23, Jun 25-

434 Jul 1 and Jul 3. For each day, only the daytime chemistry (5:00 AM - 7:00 PM) was
435 simulated, when photochemical reactivity was high. The observed IN and MVK+MACR
436 concentrations at 5:00 AM were used as the initial concentrations for simulations. For
437 isoprene, α -pinene, β -pinene, limonene, NO, NO₂, OH, HO₂, and O₃, the model
438 concentrations were constrained to observations for the entire modeling period. The
439 branching ratio for IN formation resulting from the isoprene RO₂ + NO reaction was set
440 to 0.09 for all isomers, which is based on our measured 9% yield from the chamber
441 experiments. As mentioned above, to avoid the complication in the simulation of the
442 absolute concentration variability from transport and changing boundary layer height, we
443 compared the simulated and observed $[IN]/([MVK]+[MACR])$ ratio to evaluate the
444 model.

445 Figure 8a shows the temporal profiles of the modeled and observed
446 $[IN]/([MVK]+[MACR])$ ratio for the selected 12 days. To gain a statistical overview of
447 the model and observation comparison, the 12-day average was calculated (Figure 8b).
448 The 0D model generally agrees with the observed ratio, lending support to the IN
449 branching ratio determined in the chamber experiments. However, the morning increase
450 was underestimated by the model on certain days (Jun 14, Jun 16, Jun 29, Jul 1 and Jul 3),
451 while on other days (Jun 23 and Jun 25-Jun 27), the decrease rate for the
452 $[IN]/([MVK]+[MACR])$ ratio was underestimated in the afternoon. Since the IN yield
453 applied in the 0D model has +36%/-33% uncertainty, a sensitivity test on the yield was
454 performed. As shown in Figure 8c, the simulated $[IN]/([MVK]+[MACR])$ ratio is highly
455 sensitive to the yield used in the model. The 6% yield significantly underestimated the
456 ratio in the morning, and the 12% yield significantly overestimated the ratio in the
457 afternoon.

458 **4 Discussion**

459 **4.1 Model-observation comparison for SOAS data**

460 As shown in Figure 8c, the modeled results deviated from observations from 10:00 AM
461 to 12:00 PM for all the three yields applied. During this period, the simulated
462 $[IN]/([MVK]+[MACR])$ ratio decreased slowly, but the observed ratio dropped rapidly.

463 The fast decrease in the $[IN]/([MVK]+[MACR])$ ratio implies either fast production of
464 MVK+MACR, or fast consumption of IN. In terms of fast production of MVK+MACR,
465 the formation of MVK+MACR from OH and O₃ have been characterized in the model,
466 and the model was capable of simulating MVK+MACR concentration to within
467 measurement uncertainty for the chamber experiments (Supplement 3.1). Therefore, the
468 discrepancy between model and observation is potentially associated with underestimated
469 loss rate of IN. The model results with the 6% yield were lower than observations,
470 despite potential underestimated IN loss rate, so a higher yield (9-12%) may be more
471 accurate to describe the branching ratio for isoprene RO₂+NO reaction.

472 The model overestimation in the afternoon can be caused collectively by measurement
473 uncertainties for model input, uncertainties in the IN loss rates for OH oxidation and
474 deposition, uncertainties in ambient IN (25%) and MVK+MACR (40%) measurement,
475 and other missing IN loss processes. A recent study found that isoprene hydroperoxide
476 (ISOPOOH) could interfere with MVK and MACR measurement when standard PTR-
477 MS and GC methods are used (Rivera-Rios et al., 2014). We found that the model
478 appeared to agree better with observations in the afternoon, if the ISOPOOH+IEPOX
479 concentration was subtracted from the MVK+MACR measurement data (Figure 8d).
480 However, the exact influence of ISOPOOH+IEPOX on the observations of
481 MVK+MACR is unclear, as the ISOPOOH conversion efficiency is highly dependent on
482 instrumental sampling configuration, and the interference of IEPOX has not been
483 characterized.

484 We also considered that an underestimated IN photolysis rate could be one of the reasons
485 for the model-observation discrepancy. The photolysis rate for IN was set to be identical
486 to the photolysis rate for alkyl nitrates in MCMv3.2, but IN isomers have double bonds
487 and hydroxyl groups, which could increase the IN absorption cross section and enhance
488 the photolytic reactivity for IN. When the IN photolysis rate was increased by 5 times for
489 the 9% yield, or 12.5 times for the 12% yield, the simulated $[IN]/([MVK]+[MACR])$
490 ratio was brought closer to observation in the afternoon, but the IN loss rate still appeared
491 underestimated between 10:00 AM and 12:00 PM (Figure 8e). When the higher
492 photolysis rates were applied, the simulated IN loss to photolysis could contribute up to
493 30% (9% yield case) or 50% (12% yield case) of total IN loss. Since no experimental

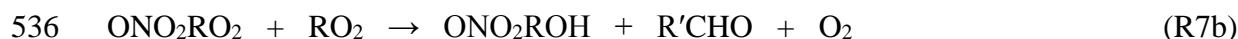
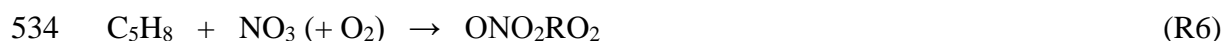
494 data were available on the absorption cross spectrum and quantum yield for IN, large
495 photo-dissociation rate coefficients are purely hypothetical. While photolysis may be a
496 significant IN sink in the ambient environment, its contribution to IN loss in chamber
497 experiments is negligible, as the lamp radiation was ~10% of solar radiation and the
498 durations of the chamber experiments were short. Therefore, no correction for the
499 photolytic loss was made for the IN measurement performed in chamber experiments.

500 Despite the discrepancy in absolute values, the simulated $[IN]/([MVK]+[MACR])$ ratios
501 all peaked in the morning, consistent with observation. The peak signifies the time when
502 the IN loss rate started to exceed the IN production rate. As the OH-loss lifetime of IN
503 decreased from 8:00 AM to 1:00 PM, the IN production rate (Figure 7b) remained
504 constant during this time. Although isoprene and OH concentrations were both greater
505 after the noontime, the IN production rate did not increase, due to the small γ value.
506 Therefore, the morning IN peak can be attributed to the combined effects of slow IN
507 production and fast IN consumption in the afternoon, with NO_x being the limiting factor
508 for IN production during this field study.

509 Although the simulated $[IN]/([MVK]+[MACR])$ ratios all peaked in the morning, they
510 peaked one hour later than the observed ratio (Figure 8c). In addition, the modeled ratio
511 had a smaller growth rate than the observed ratio between 7:00 AM and 9:00 AM,
512 regardless of the IN yield and IN loss rate applied (Figure 8c and 8d). This
513 underprediction implies an unknown source of IN, and we can hypothesize that it was
514 caused by downward mixing of the RL IN, as the fast morning increase of IN coincided
515 with inversion breakup. By combining the observations of IN and MVK+MACR during
516 SOAS and the results from the 0D model, we can calculate the growth rate of ambient IN
517 concentration caused solely by isoprene photochemistry in the daytime (Supplement Sect.
518 7). This photochemical IN growth rate was compared with the observed IN growth rate,
519 and from that we estimate that downward mixing can contribute to $27(\pm 16)\%$ of the fast
520 IN increase in the morning, where the large uncertainty originates from the uncertainty in
521 the IN yield.

522 The residual layer IN concentration before mixing (6:00 AM) was estimated with the 0D
523 model, using the same initial input as the ground-level observation on the previous day at

524 8:00 PM. The chemical processes involved are IN production from isoprene oxidation by
525 NO₃ (R5 and R6b) and IN consumption by OH, O₃ and NO₃. Based on our model
526 calculation, the steady-state NO₃ concentration at night was on the order of 1×10⁶
527 molecules cm⁻³. Nighttime OH was generated through BVOC ozonolysis, and the
528 simulated concentration was on the order of 5×10⁴ molecules cm⁻³. Even though the OH
529 concentration was very low at night, it was still the dominant IN loss pathway, because of
530 the fast IN+OH reaction rate constants. It is worth noting that RO₂ produced from
531 isoprene + NO₃ (R6) also has competing loss channels for reaction with RO₂ (R7) and
532 with HO₂ (R8). Therefore, only a fraction of the isoprene nitrooxy peroxy radicals
533 (ONO₂RO₂) can react with other peroxy radicals to produce IN through reaction R7b.



538 Figure 9 shows the simulated IN concentration in the RL and IN observed near ground
539 before dawn, assuming the RL was completely stable at night with no depositional loss
540 for IN from the RL. The simulated IN concentration in the RL before dawn was greater
541 than the concentrations measured at ground level by up to one order of magnitude,
542 indicating the IN stored in the RL overnight may be a significant ground level IN source
543 during inversion breakup. This high IN concentration above the NBL is the result of IN
544 produced during the previous day, which is present with the high concentration in the RL
545 as it is formed, and zero deposition removal overnight. The NO₂ concentration is low
546 when the RL is formed at sunset, so contribution from IN production through NO₃
547 chemistry is small (1-10ppt), a minor fraction compared with the concentration of IN
548 already present in the RL in the evening. Isoprene-NO₃ chemistry can generate IN
549 isomers with a different isomeric distribution. Since IN production from this reaction
550 scheme is small, no sensitivity correction was performed to account for the changes in
551 isomer distribution when RL IN mixed with ground-level IN in the morning.

552 The calculated residual layer IN does not take into account the altitude-dependent IN
553 concentration caused by OH oxidation, as well as possible IN concentration change
554 caused by advection. Therefore, the actual IN concentration may be very different from
555 the calculated results. This is reflected in a comparison of the large RL IN excess relative
556 to surface IN on Jun 26 and 27 (Figure 9), with simultaneous model overprediction of
557 daytime IN on these two days (Figure 8a). Hence, detailed three-dimensional chemical
558 transport models are needed to fully elucidate the production and storage mechanisms of
559 IN in the ambient environment.

560 **4.2 High-NO_x and low-NO_x chemistry during SOAS**

561 OH oxidation was the most important daytime sink for BVOCs during SOAS. As the γ
562 value decreased from 0.95 at 7:00 AM to 0.3 at 1:00 PM (Figure 7b), the BVOC-derived
563 RO₂ radicals are expected to undergo both NO (high NO_x) and HO₂ (low NO_x) reaction
564 pathways throughout the day. For isoprene, the presence of the two reaction schemes was
565 signified by the oxidation products, with IN peaking in the morning and ISOPOOH and
566 IEPOX peaking in the afternoon (Figure 10).

567 As IN was consumed by OH, it would also undertake both NO and HO₂ reaction
568 pathways. Since the highest OH concentrations (1:00 PM) were accompanied with a
569 small γ value (~0.3, Figure 7b), significant amount of IN would be oxidized following the
570 HO₂ pathway. A possible reaction scheme is illustrated in Figure 11 with 1,2-IN as an
571 example.

572 Experimental studies by Jacobs et al. (2014) suggest that OH addition to IN can invoke
573 IEPOX formation with a yield of 13% at atmospheric pressure, which simultaneously
574 releases NO₂. Although IEPOX can be produced from IN oxidation, the ISOPOOH
575 pathway was still the dominant IEPOX precursor during this study, due to the higher
576 concentrations of ISOPOOH and its higher yield for IEPOX (~70-80%) (St. Clair et al.,
577 2015). For RO₂ radicals produced from OH addition to IN, 30% will react with NO and
578 70% will react with HO₂ for a γ value of 0.3 at 1:00 PM.

579 For the RO₂+NO reaction, Lee et al. (2014b) observed the formation of dinitrate for δ
580 isomers of IN and estimated a branching ratio of less than 18% for β -4,3-IN based on

581 missing carbon in the gas phase. The RO radicals from the RO₂+NO reaction will
582 dissociate to make either MACR nitrate or lose NO₂ to form hydroxyacetone and
583 glycoaldehyde. Both Jacobs et al. (2014) and Lee et al. (2014b) reported MACR nitrate
584 being the dominant product with an overall yield of 70%, thus making the corresponding
585 branching ratio for the RO radical to be around 80%.

586 The RO₂+HO₂ products from IN oxidation are less understood. Alkyl peroxy radical
587 reaction with HO₂ can undergo two reaction channels to afford either hydroperoxide or
588 RO radical and OH. The branching ratio is highly structure dependent. Simple alkyl
589 peroxy radicals, such as CH₃CH₂O₂, can form hydroperoxide with almost unity yield
590 (Hasson et al., 2004). However, for peroxy radicals with β carbonyl groups, such as
591 RC(O)CH₂O₂, the branching ratio for the OH formation pathway is more than 60%
592 (Hasson et al., 2012; Hasson et al., 2004). The β carbonyl oxygen can stabilize the
593 reaction intermediate through internal hydrogen bonding, thus making the reaction favor
594 the formation of OH and RO (Hasson et al., 2005). The RO₂ from IN oxidation has a β-
595 OH group and a β-NO₃ group, both capable of forming internal hydrogen bonding with
596 the hydrogen of HO₂. Therefore, formation of OH and RO radicals may be a significant
597 reaction channel when the RO₂ radicals derived from IN react with HO₂. The closed-shell
598 product from the RO₂+HO₂ reaction is dihydroxy hydroperoxy nitrate (DHHPN). This
599 compound has not been identified in any laboratory studies. However, Lee et al. (2015)
600 found a significant amount of compounds with the corresponding molecular formula of
601 C₅H₁₁O₇N in the aerosol phase during SOAS, which suggests that hydroperoxide
602 formation and aerosol uptake could be an important sink for IN.

603 A range can be estimated for the NO₂ recycling efficiency for IN oxidation, as the
604 detailed RO₂+HO₂ reaction mechanism is unclear. If RO₂+HO₂ reaction forms only
605 hydroperoxide, the NO₂ yield from IN oxidation will be 17%. If RO₂+HO₂ reaction only
606 undergoes the radical formation channel, the NO₂ yield will be 30%, and the major
607 products of IN oxidation are highly oxidized secondary nitrates.

608 **5 Summary and atmospheric implications**

609 Our chamber experiments indicate a 9(+4/-3)% nitrate yield from isoprene
610 hydroxyperoxy radical reaction with NO. The product yield provides a more reliable

611 groundwork for future modeling studies on the interplay of isoprene oxidation, NO_x
612 cycling, and tropospheric O₃ production.

613 Our field measurements and model simulations suggest that in the southeast US,
614 formation of organic nitrates in the boundary layer is controlled by the availability of
615 NO_x. During the SOAS field study, when isoprene was oxidized by OH addition, the NO
616 peak in the morning on average consumed 95% of the isoprene RO₂ to form high NO_x
617 photooxidation products such as IN, MVK and MACR. As the NO_x concentration
618 decreased during the day, the RO₂+HO₂ reactions became more important, and by ~1:00
619 PM only 30% of the RO₂ react with NO, and thus only 2.7% of the RO₂ would form
620 organic nitrates. The high NO_x concentration in the early morning caused an early IN
621 maximum at 10:00 AM, a combined result of slow afternoon IN production with limited
622 NO_x, and fast IN consumption due to peak radiation and fast OH production in the
623 afternoon. By comparing simulation results with observations, we estimate the inversion
624 breakup after sunrise may contribute to 27(±16)% of the rapid IN increase in the
625 morning. The observed daytime IN loss can be approximated with the current
626 understanding of IN oxidation reactions and dry deposition, but some discrepancies still
627 exist, which could be caused by other less studied loss pathways, such as nitrate
628 photolysis. Aerosol uptake could also be an IN sink, but the contribution is expected to be
629 small (Surratt et al., 2010b). Observations during SOAS suggest that the isoprene-derived
630 SOA components were associated with IEPOX and more oxidized organic nitrates, not
631 the first-generation hydroxynitrates (Xu et al., 2015b; Lee et al., 2015).

632 While IN were produced and destroyed in the morning through high NO_x chemistry, a
633 major portion of the afternoon IN oxidation process involved low NO_x chemistry, which
634 could yield products such as the highly oxidized hydroperoxide DHHPN. DHHPN is
635 expected to have very low vapor pressure and undergo fast dry deposition and aerosol
636 partitioning, possibly followed by hydrolysis and formation of NO₃⁻ and trihydroxy
637 hydroperoxide. This process removes NO_x from the atmosphere and helps to shift the
638 photochemical processes further toward the low NO_x regime, forming a positive feedback
639 mechanism to reduce the atmospheric NO_x concentration. However, more experimental
640 studies are required to elucidate the detailed mechanism for the RO₂+HO₂ reactions.

641 During the past 15 years, NO_x emissions in the southeastern US have decreased by more
642 than 50% (Hidy et al., 2014). As more effort is devoted to controlling anthropogenic
643 emissions, the BVOC oxidation processes will start to shift further toward the low NO_x
644 regime. Isoprene products resulting from oxidation in the low NO_x condition, such as
645 IEPOX, are more prone to reactive uptake and thus contribute more effectively to the
646 growth of SOA than IN (Xu et al., 2015a; Surratt et al., 2010a; Nguyen et al., 2014a),
647 indicating potentially higher SOA burdens from isoprene chemistry in the future. The low
648 NO_x photochemistry is often complicated by radical reactions including intramolecular
649 H-shift and autoxidation (So et al., 2014; Peeters et al., 2014; Savee et al., 2015; Crouse
650 et al., 2013), so more theoretical and experimental studies of the fundamental reaction
651 kinetics are needed to unravel the complete BVOC oxidation mechanism. The
652 photochemical reactions that involve both the high NO_x and low NO_x pathways can yield
653 new highly-oxidized multi-functional nitrate products. Identification, quantification and
654 study of the chemistry of these organic nitrates is essential to understand the fate of NO_x.
655 As the highly-oxidized compounds, such as DHHPN and dinitrate, tend to partition into
656 the aerosol phase, it will be a challenge for the development of analytical techniques to
657 investigate their aging process in the particle phase and their role in the NO_x cycle.

658 **Acknowledgement**

659 We thank the organizers of the SOAS study, especially Dr. Ann Marie Carlton. We
660 appreciate help from Dr. Jozef Peeters at University of Leuven in elucidating the
661 uncertainties associated with the current LIM1 mechanism. We acknowledge funding
662 from the National Science Foundation (NSF) grant 1228496 and US Environmental
663 Protection Agency (EPA) STAR grant 83540901.

664 **References**

- 665 Atkinson, R., Aschmann, S. M., Carter, W. P. L., Winer, A. M., and Pitts, J. N.: Alkyl nitrate
666 formation from the nitrogen oxide (NO_x)-air photooxidations of C2-C8 n-alkanes, *The Journal of*
667 *Physical Chemistry*, 86, 4563-4569, 10.1021/j100220a022, 1982.
- 668 Bates, K. H., Crouse, J. D., St Clair, J. M., Bennett, N. B., Nguyen, T. B., Seinfeld, J. H., Stoltz, B.
669 M., and Wennberg, P. O.: Gas phase production and loss of isoprene epoxydiols, *The journal of*
670 *physical chemistry. A*, 118, 1237-1246, 10.1021/jp4107958, 2014.
- 671 Beaver, M. R., St Clair, J. M., Paulot, F., Spencer, K. M., Crouse, J. D., LaFranchi, B. W., Min, K. E.,
672 Pusede, S. E., Wooldridge, P. J., Schade, G. W., Park, C., Cohen, R. C., and Wennberg, P. O.:

673 Importance of biogenic precursors to the budget of organic nitrates: observations of
674 multifunctional organic nitrates by CIMS and TD-LIF during BEARPEX 2009, *Atmospheric*
675 *Chemistry and Physics*, 12, 5773-5785, 10.5194/acp-12-5773-2012, 2012.

676 Carter, W. P. L., and Atkinson, R.: Development and evaluation of a detailed mechanism for the
677 atmospheric reactions of isoprene and NO_x, *International Journal of Chemical Kinetics*, 28, 497-
678 530, 10.1002/(SICI)1097-4601(1996)28:7<497::AID-KIN4>3.0.CO;2-Q, 1996.

679 Chen, X., Hulbert, D., and Shepson, P. B.: Measurement of the organic nitrate yield from OH
680 reaction with isoprene, *Journal of Geophysical Research*, 103, 25563, 10.1029/98jd01483, 1998.

681 Crouse, J. D., McKinney, K. A., Kwan, A. J., and Wennberg, P. O.: Measurement of Gas-Phase
682 Hydroperoxides by Chemical Ionization Mass Spectrometry, *Analytical chemistry*, 78, 6726-6732,
683 10.1021/ac0604235, 2006.

684 Crouse, J. D., Paulot, F., Kjaergaard, H. G., and Wennberg, P. O.: Peroxy radical isomerization in
685 the oxidation of isoprene, *Physical chemistry chemical physics : PCCP*, 13, 13607-13613,
686 10.1039/c1cp21330j, 2011.

687 Crouse, J. D., Nielsen, L. B., Jørgensen, S., Kjaergaard, H. G., and Wennberg, P. O.: Autoxidation
688 of Organic Compounds in the Atmosphere, *The Journal of Physical Chemistry Letters*, 4, 3513-
689 3520, 10.1021/jz4019207, 2013.

690 Day, D. A., Wooldridge, P. J., Dillon, M. B., Thornton, J. A., and Cohen, R. C.: A thermal
691 dissociation laser-induced fluorescence instrument for in situ detection of NO₂, peroxy nitrates,
692 alkyl nitrates, and HNO₃, *Journal of Geophysical Research: Atmospheres*, 107, ACH 4-1-ACH 4-
693 14, 10.1029/2001JD000779, 2002.

694 Fan, J., and Zhang, R.: Atmospheric Oxidation Mechanism of Isoprene, *Environmental Chemistry*,
695 1, 140, 10.1071/en04045, 2004.

696 Giacomelli, P., Ford, K., Espada, C., and Shepson, P. B.: Comparison of the measured and
697 simulated isoprene nitrate distributions above a forest canopy, *Journal of Geophysical Research*,
698 110, D01304, 10.1029/2004jd005123, 2005.

699 Gilman, J. B., Burkhardt, J. F., Lerner, B. M., Williams, E. J., Kuster, W. C., Goldan, P. D., Murphy, P.
700 C., Warneke, C., Fowler, C., Montzka, S. A., Miller, B. R., Miller, L., Oltmans, S. J., Ryerson, T. B.,
701 Cooper, O. R., Stohl, A., and de Gouw, J. A.: Ozone variability and halogen oxidation within the
702 Arctic and sub-Arctic springtime boundary layer, *Atmos. Chem. Phys.*, 10, 10223-10236,
703 10.5194/acp-10-10223-2010, 2010.

704 Grosjean, D., Williams, E. L., and Grosjean, E.: Atmospheric chemistry of isoprene and of its
705 carbonyl products, *Environmental science & technology*, 27, 830-840, 10.1021/es00042a004,
706 1993.

707 Grossenbacher, J. W., Couch, T., Shepson, P. B., Thornberry, T., Witmer-Rich, M., Carroll, M. A.,
708 Faloon, I., Tan, D., Brune, W., Ostling, K., and Bertman, S.: Measurements of isoprene nitrates
709 above a forest canopy, *Journal of Geophysical Research*, 106, 24429, 10.1029/2001jd900029,
710 2001.

711 Grossenbacher, J. W., Barkat Jr, D. J., Shepson, P. B., Carroll, M. A., Olszyna, K., and Apel, E.: A
712 comparison of isoprene nitrate concentrations at two forest-impacted sites, *Journal of*
713 *Geophysical Research: Atmospheres*, 109, D11311, 10.1029/2003JD003966, 2004.

714 Guenther, A., Karl, T., Harley, P., Wiedinmyer, C., Palmer, P. I., and Geron, C.: Estimates of global
715 terrestrial isoprene emissions using MEGAN (Model of Emissions of Gases and Aerosols from
716 Nature), *Atmos. Chem. Phys.*, 6, 3181-3210, 10.5194/acp-6-3181-2006, 2006.

717 Hao, C., Shepson, P. B., Drummond, J. W., and Muthuramu, K.: Gas Chromatographic Detector
718 for Selective and Sensitive Detection of Atmospheric Organic Nitrates, *Analytical chemistry*, 66,
719 3737-3743, 10.1021/ac00093a032, 1994.

720 Hartsell, B. E., Aneja, V. P., and Lonneman, W. A.: Relationships between peroxyacetyl nitrate,
721 O₃, and NO_y at the rural Southern Oxidants Study site in central Piedmont, North Carolina, site
722 SONIA, *Journal of Geophysical Research: Atmospheres*, 99, 21033-21041, 10.1029/94JD01021,
723 1994.

724 Harwood, L. M., Casy, G., and Sherlock, J.: A Simple Laboratory Procedure for Preparation of (1-
725 Methylene)oxirane (3,4-Epoxyisoprene), *Synthetic Communications*, 20, 1287-1292,
726 10.1080/00397919008052839, 1990.

727 Hasson, A. S., Tyndall, G. S., and Orlando, J. J.: A Product Yield Study of the Reaction of HO₂
728 Radicals with Ethyl Peroxy (C₂H₅O₂), Acetyl Peroxy (CH₃C(O)O₂), and Acetyl Peroxy
729 (CH₃C(O)CH₂O₂) Radicals, *The Journal of Physical Chemistry A*, 108, 5979-5989,
730 10.1021/jp048873t, 2004.

731 Hasson, A. S., Kuwata, K. T., Arroyo, M. C., and Petersen, E. B.: Theoretical studies of the
732 reaction of hydroperoxy radicals (HO₂) with ethyl peroxy (CH₃CH₂O₂), acetyl peroxy
733 (CH₃C(O)O₂), and acetyl peroxy (CH₃C(O)CH₂O₂) radicals, *Journal of Photochemistry and
734 Photobiology A: Chemistry*, 176, 218-230, <http://dx.doi.org/10.1016/j.jphotochem.2005.08.012>,
735 2005.

736 Hasson, A. S., Tyndall, G. S., Orlando, J. J., Singh, S., Hernandez, S. Q., Campbell, S., and Ibarra, Y.:
737 Branching ratios for the reaction of selected carbonyl-containing peroxy radicals with
738 hydroperoxy radicals, *The journal of physical chemistry. A*, 116, 6264-6281, 10.1021/jp211799c,
739 2012.

740 Hastie, D. R., Shepson, P. B., Sharma, S., and Schiff, H. I.: The influence of the nocturnal
741 boundary layer on secondary trace species in the atmosphere at Dorset, Ontario, *Atmospheric
742 Environment. Part A. General Topics*, 27, 533-541, [http://dx.doi.org/10.1016/0960-
743 1686\(93\)90210-P](http://dx.doi.org/10.1016/0960-1686(93)90210-P), 1993.

744 Hidy, G. M., Blanchard, C. L., Baumann, K., Edgerton, E., Tanenbaum, S., Shaw, S., Knipping, E.,
745 Tombach, I., Jansen, J., and Walters, J.: Chemical climatology of the southeastern United States,
746 1999–2013, *Atmospheric Chemistry and Physics*, 14, 11893-11914, 10.5194/acp-14-
747 11893-2014, 2014.

748 Horowitz, L. W., Fiore, A. M., Milly, G. P., Cohen, R. C., Perring, A., Wooldridge, P. J., Hess, P. G.,
749 Emmons, L. K., and Lamarque, J.-F.: Observational constraints on the chemistry of isoprene
750 nitrates over the eastern United States, *Journal of Geophysical Research*, 112, D12S08,
751 10.1029/2006jd007747, 2007.

752 Hu, K. S., Darer, A. I., and Elrod, M. J.: Thermodynamics and kinetics of the hydrolysis of
753 atmospherically relevant organonitrates and organosulfates, *Atmospheric Chemistry and
754 Physics*, 11, 8307-8320, 10.5194/acp-11-8307-2011, 2011.

755 Jacobs, M. I., Burke, W. J., and Elrod, M. J.: Kinetics of the reactions of isoprene-derived
756 hydroxynitrates: gas phase epoxide formation and solution phase hydrolysis, *Atmospheric*
757 *Chemistry and Physics*, 14, 8933-8946, 10.5194/acp-14-8933-2014, 2014.

758 Jenkin, M. E., Saunders, S. M., and Pilling, M. J.: The tropospheric degradation of volatile organic
759 compounds: a protocol for mechanism development, *Atmospheric Environment*, 31, 81-104,
760 [http://dx.doi.org/10.1016/S1352-2310\(96\)00105-7](http://dx.doi.org/10.1016/S1352-2310(96)00105-7), 1997.

761 Kwan, A. J., Chan, A. W. H., Ng, N. L., Kjaergaard, H. G., Seinfeld, J. H., and Wennberg, P. O.:
762 Peroxy radical chemistry and OH radical production during the NO₃-initiated
763 oxidation of isoprene, *Atmospheric Chemistry and Physics*, 12, 7499-7515, 10.5194/acp-12-
764 7499-2012, 2012.

765 Lee, B. H., Lopez-Hilfiker, F. D., Mohr, C., Kurtén, T., Worsnop, D. R., and Thornton, J. A.: An
766 Iodide-Adduct High-Resolution Time-of-Flight Chemical-Ionization Mass Spectrometer:
767 Application to Atmospheric Inorganic and Organic Compounds, *Environmental science &*
768 *technology*, 48, 6309-6317, 10.1021/es500362a, 2014a.

769 Lee, B. H., Mohr, C., Lopez-Hilfiker, F. D., D'Ambro1, E. L., Lutz, A., Hallquist, M., Lee, L., Romer,
770 P., Cohen, R. C., Iyer, S., Kurten, T., Hu, W. W., Day, D. A., Campuzano-Jost, P., Jimenez, J. L., Xu,
771 L., Ng, N. L., Wild, R. J., Brown, S. S., Koss, A., Gouw, J. d., Olson, K., Goldstein, A. H., Seco, R.,
772 Kim, S., McAvey, K., Shepson, P. B., Baumann, K., Edgerton, E. S., Nguyen, T. B., Wennberg, P. O.,
773 Liu, J., Shilling, J. E., and Thornton, J. A.: Highly functionalized particle-phase organic nitrates
774 observed in the Southeastern U.S.: contribution to secondary organic aerosol and reactive
775 nitrogen budgets, in preparation, 2015.

776 Lee, L., Teng, A. P., Wennberg, P. O., Crouse, J. D., and Cohen, R. C.: On rates and mechanisms
777 of OH and O₃ reactions with isoprene-derived hydroxy nitrates, *The journal of physical*
778 *chemistry. A*, 118, 1622-1637, 10.1021/jp4107603, 2014b.

779 Liao, J., Sihler, H., Huey, L. G., Neuman, J. A., Tanner, D. J., Friess, U., Platt, U., Flocke, F. M.,
780 Orlando, J. J., Shepson, P. B., Beine, H. J., Weinheimer, A. J., Sjostedt, S. J., Nowak, J. B., Knapp,
781 D. J., Staebler, R. M., Zheng, W., Sander, R., Hall, S. R., and Ullmann, K.: A comparison of Arctic
782 BrO measurements by chemical ionization mass spectrometry and long path-differential optical
783 absorption spectroscopy, *Journal of Geophysical Research*, 116, D00R02,
784 10.1029/2010jd014788, 2011.

785 Liu, Y. J., Herdinger-Blatt, I., McKinney, K. A., and Martin, S. T.: Production of methyl vinyl
786 ketone and methacrolein via the hydroperoxyl pathway of isoprene oxidation, *Atmospheric*
787 *Chemistry and Physics*, 13, 5715-5730, 10.5194/acp-13-5715-2013, 2013.

788 Lockwood, A. L., Shepson, P. B., Fiddler, M. N., and Alaghmand, M.: Isoprene nitrates:
789 preparation, separation, identification, yields, and atmospheric chemistry, *Atmospheric*
790 *Chemistry and Physics*, 10, 6169-6178, 10.5194/acp-10-6169-2010, 2010.

791 Madronich, S., and Flocke, S.: The role of solar radiation in atmospheric chemistry, in: *Handbook*
792 *of Environmental Chemistry*, edited by: Boule, P., Springer-Verlag, Heidelberg, 1-26, 1998.

793 Mielke, L. H., Pratt, K. A., Shepson, P. B., McLuckey, S. A., Wisthaler, A., and Hansel, A.:
794 Quantitative Determination of Biogenic Volatile Organic Compounds in the Atmosphere Using
795 Proton-Transfer Reaction Linear Ion Trap Mass Spectrometry, *Analytical chemistry*, 82, 7952-
796 7957, 10.1021/ac1014244, 2010.

797 Misztal, P. K., Guenther, A., and Goldstein, A. H.: Flux observations of isoprene oxidation
798 products above forests point to potential role of leaf-surface reactions, In preparation.

799 Neu, U., Künzle, T., and Wanner, H.: On the relation between ozone storage in the residual layer
800 and daily variation in near-surface ozone concentration — A case study, *Boundary-Layer*
801 *Meteorol*, 69, 221-247, 10.1007/BF00708857, 1994.

802 Nguyen, T. B., Coggon, M. M., Bates, K. H., Zhang, X., Schwantes, R. H., Schilling, K. A., Loza, C. L.,
803 Flagan, R. C., Wennberg, P. O., and Seinfeld, J. H.: Organic aerosol formation from the reactive
804 uptake of isoprene epoxydiols (IEPOX) onto non-acidified inorganic seeds, *Atmospheric*
805 *Chemistry and Physics*, 14, 3497-3510, 10.5194/acp-14-3497-2014, 2014a.

806 Nguyen, T. B., Crounse, J. D., Schwantes, R. H., Teng, A. P., Bates, K. H., Zhang, X., St. Clair, J. M.,
807 Brune, W. H., Tyndall, G. S., Keutsch, F. N., Seinfeld, J. H., and Wennberg, P. O.: Overview of the
808 Focused Isoprene eXperiment at the California Institute of Technology (FIXCIT): mechanistic
809 chamber studies on the oxidation of biogenic compounds, *Atmospheric Chemistry and Physics*,
810 14, 13531-13549, 10.5194/acp-14-13531-2014, 2014b.

811 Nguyen, T. B., Crounse, J. D., Teng, A. P., St Clair, J. M., Paulot, F., Wolfe, G. M., and Wennberg,
812 P. O.: Rapid deposition of oxidized biogenic compounds to a temperate forest, *Proceedings of*
813 *the National Academy of Sciences of the United States of America*, 10.1073/pnas.1418702112,
814 2015.

815 O'Brien, J. M., Shepson, P. B., Muthuramu, K., Hao, C., Niki, H., Hastie, D. R., Taylor, R., and
816 Roussel, P. B.: Measurements of alkyl and multifunctional organic nitrates at a rural site in
817 Ontario, *Journal of Geophysical Research: Atmospheres*, 100, 22795-22804,
818 10.1029/94JD03247, 1995.

819 Patchen, A. K., Pennino, M. J., Kiep, A. C., and Elrod, M. J.: Direct kinetics study of the product-
820 forming channels of the reaction of isoprene-derived hydroxyperoxy radicals with NO,
821 *International Journal of Chemical Kinetics*, 39, 353-361, 10.1002/kin.20248, 2007.

822 Paulot, F., Crounse, J. D., Kjaergaard, H. G., Kroll, J. H., Seinfeld, J. H., and Wennberg, P. O.:
823 Isoprene photooxidation: new insights into the production of acids and organic nitrates, *Atmos.*
824 *Chem. Phys.*, 9, 1479-1501, 10.5194/acp-9-1479-2009, 2009.

825 Paulot, F., Henze, D. K., and Wennberg, P. O.: Impact of the isoprene photochemical cascade on
826 tropical ozone, *Atmospheric Chemistry and Physics*, 12, 1307-1325, 10.5194/acp-12-1307-2012,
827 2012.

828 Peeters, J., Nguyen, T. L., and Vereecken, L.: HOx radical regeneration in the oxidation of
829 isoprene, *Physical chemistry chemical physics : PCCP*, 11, 5935-5939, 10.1039/b908511d, 2009.

830 Peeters, J., Müller, J.-F., Stavrou, T., and Nguyen, V. S.: Hydroxyl Radical Recycling in Isoprene
831 Oxidation Driven by Hydrogen Bonding and Hydrogen Tunneling: The Upgraded LIM1
832 Mechanism, *The Journal of Physical Chemistry A*, 118, 8625-8643, 10.1021/jp5033146, 2014.

833 Perring, A. E., Wisthaler, A., Graus, M., Wooldridge, P. J., Lockwood, A. L., Mielke, L. H., Shepson,
834 P. B., Hansel, A., and Cohen, R. C.: A product study of the isoprene+NO₃ reaction, *Atmos. Chem.*
835 *Phys.*, 9, 4945-4956, 10.5194/acp-9-4945-2009, 2009.

836 Rindelaub, J. D., McAvey, K. M., and Shepson, P. B.: The photochemical production of organic
837 nitrates from α -pinene and loss via acid-dependent particle phase hydrolysis, *Atmospheric*
838 *Environment*, 100, 193-201, <http://dx.doi.org/10.1016/j.atmosenv.2014.11.010>, 2015.

839 Rivera-Rios, J. C., Nguyen, T. B., Crouse, J. D., Jud, W., St. Clair, J. M., Mikoviny, T., Gilman, J. B.,
840 Lerner, B. M., Kaiser, J. B., de Gouw, J., Wisthaler, A., Hansel, A., Wennberg, P. O., Seinfeld, J. H.,
841 and Keutsch, F. N.: Conversion of hydroperoxides to carbonyls in field and laboratory
842 instrumentation: Observational bias in diagnosing pristine versus anthropogenically controlled
843 atmospheric chemistry, *Geophysical Research Letters*, n/a-n/a, 10.1002/2014gl061919, 2014.

844 Rollins, A. W., Kiendler-Scharr, A., Fry, J. L., Brauers, T., Brown, S. S., Dorn, H. P., Dubé, W. P.,
845 Fuchs, H., Mensah, A., Mentel, T. F., Rohrer, F., Tillmann, R., Wegener, R., Wooldridge, P. J., and
846 Cohen, R. C.: Isoprene oxidation by nitrate radical: alkyl nitrate and secondary organic aerosol
847 yields, *Atmos. Chem. Phys.*, 9, 6685-6703, 10.5194/acp-9-6685-2009, 2009.

848 Rollins, A. W., Smith, J. D., Wilson, K. R., and Cohen, R. C.: Real Time In Situ Detection of Organic
849 Nitrates in Atmospheric Aerosols, *Environmental science & technology*, 44, 5540-5545,
850 10.1021/es100926x, 2010.

851 Saunders, S. M., Jenkin, M. E., Derwent, R. G., and Pilling, M. J.: Protocol for the development of
852 the Master Chemical Mechanism, MCM v3 (Part A): tropospheric degradation of non-aromatic
853 volatile organic compounds, *Atmos. Chem. Phys.*, 3, 161-180, 10.5194/acp-3-161-2003, 2003.

854 Savee, J. D., Papajak, E., Rotavera, B., Huang, H., Eskola, A. J., Welz, O., Sheps, L., Taatjes, C. A.,
855 Zádor, J., and Osborn, D. L.: Direct observation and kinetics of a hydroperoxyalkyl radical
856 (QOOH), *Science*, 347, 643-646, 10.1126/science.aaa1495, 2015.

857 So, S., Kirk, B. B., Trevitt, A. J., Wille, U., Blanksby, S. J., and da Silva, G.: Unimolecular reaction
858 chemistry of a charge-tagged beta-hydroxyperoxyl radical, *Physical Chemistry Chemical Physics*,
859 16, 24954-24964, 10.1039/C4CP02981J, 2014.

860 Sprengnether, M., Demerjian, K. L., Donahue, N. M., and Anderson, J. G.: Product analysis of the
861 OH oxidation of isoprene and 1,3-butadiene in the presence of NO, *Journal of Geophysical
862 Research*, 107, 10.1029/2001jd000716, 2002.

863 St. Clair, J. M., Rivera, J. C., Crouse, J. D., Knap, H. C., Bates, K. H., Teng, A. P., Jørgensen, S.,
864 Kjaergaard, H. G., Keutsch, F. N., and Wennberg, P. O.: Kinetics and Products of the Reaction of
865 the First-Generation Isoprene Hydroxy Hydroperoxide (ISOPOOH) with OH, *The Journal of
866 Physical Chemistry A*, 10.1021/acs.jpca.5b06532, 2015.

867 Stevens, P., L'Esperance, D., Chuong, B., and Martin, G.: Measurements of the kinetics of the
868 OH-initiated oxidation of isoprene: Radical propagation in the OH + isoprene + O₂ + NO reaction
869 system, *International Journal of Chemical Kinetics*, 31, 637-643, 10.1002/(SICI)1097-
870 4601(1999)31:9<637::AID-KIN5>3.0.CO;2-O, 1999.

871 Stutz, J.: Vertical profiles of NO₃, N₂O₅, O₃, and NO_x in the nocturnal boundary layer: 1.
872 Observations during the Texas Air Quality Study 2000, *Journal of Geophysical Research*, 109,
873 D12306, 10.1029/2003jd004209, 2004.

874 Surratt, J. D., Chan, A. W., Eddingsaas, N. C., Chan, M., Loza, C. L., Kwan, A. J., Hersey, S. P.,
875 Flagan, R. C., Wennberg, P. O., and Seinfeld, J. H.: Reactive intermediates revealed in secondary
876 organic aerosol formation from isoprene, *Proceedings of the National Academy of Sciences of
877 the United States of America*, 107, 6640-6645, 10.1073/pnas.0911114107, 2010a.

878 Surratt, J. D., Chan, A. W. H., Eddingsaas, N. C., Chan, M., Loza, C. L., Kwan, A. J., Hersey, S. P.,
879 Flagan, R. C., Wennberg, P. O., and Seinfeld, J. H.: Reactive intermediates revealed in secondary
880 organic aerosol formation from isoprene, *Proceedings of the National Academy of Sciences of
881 the United States of America*, 107, 6640-6645, 10.1073/pnas.0911114107, 2010b.

882 Teng, A. P., Crouse, J. D., Lee, L., St. Clair, J. M., Cohen, R. C., and Wennberg, P. O.: Hydroxy
 883 nitrate production in the OH-initiated oxidation of alkenes, *Atmos. Chem. Phys.*, 15, 4297-4316,
 884 10.5194/acp-15-4297-2015, 2015.

885 Tuazon, E. C., and Atkinson, R.: A product study of the gas-phase reaction of Isoprene with the
 886 OH radical in the presence of NO_x, *International Journal of Chemical Kinetics*, 22, 1221-1236,
 887 10.1002/kin.550221202, 1990.

888 Xie, Y., Paulot, F., Carter, W. P. L., Nolte, C. G., Luecken, D. J., Hutzell, W. T., Wennberg, P. O.,
 889 Cohen, R. C., and Pinder, R. W.: Understanding the impact of recent advances in isoprene
 890 photooxidation on simulations of regional air quality, *Atmospheric Chemistry and Physics*, 13,
 891 8439-8455, 10.5194/acp-13-8439-2013, 2013.

892 Xu, L., Guo, H., Boyd, C. M., Klein, M., Bougiatioti, A., Cerully, K. M., Hite, J. R., Isaacman-
 893 VanWertz, G., Kreisberg, N. M., Knote, C., Olson, K., Koss, A., Goldstein, A. H., Hering, S. V., de
 894 Gouw, J., Baumann, K., Lee, S. H., Nenes, A., Weber, R. J., and Ng, N. L.: Effects of anthropogenic
 895 emissions on aerosol formation from isoprene and monoterpenes in the southeastern United
 896 States, *Proceedings of the National Academy of Sciences of the United States of America*, 112,
 897 37-42, 10.1073/pnas.1417609112, 2015a.

898 Xu, L., Suresh, S., Guo, H., Weber, R. J., and Ng, N. L.: Aerosol characterization over the
 899 southeastern United States using high-resolution aerosol mass spectrometry: spatial and
 900 seasonal variation of aerosol composition and sources with a focus on organic nitrates,
 901 *Atmospheric Chemistry and Physics*, 15, 7307-7336, 10.5194/acp-15-7307-2015, 2015b.

902 Zhang, L., Moran, M. D., Makar, P. A., Brook, J. R., and Gong, S.: Modelling gaseous dry
 903 deposition in AURAMS: a unified regional air-quality modelling system, *Atmospheric
 904 Environment*, 36, 537-560, [http://dx.doi.org/10.1016/S1352-2310\(01\)00447-2](http://dx.doi.org/10.1016/S1352-2310(01)00447-2), 2002.

905

906

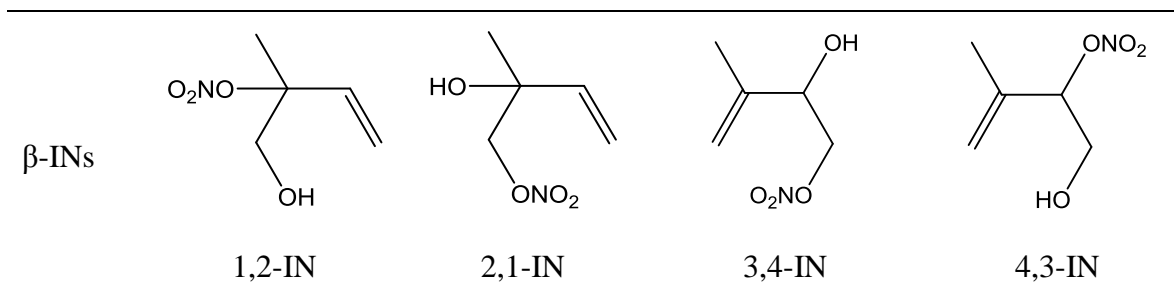
907

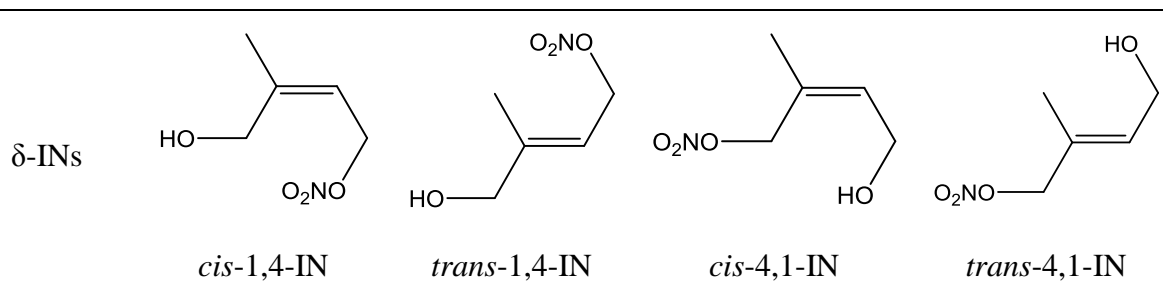
908

909

910

911 Table 1. Hydroxynitrates from OH-initiated isoprene oxidation (high NO_x).





912

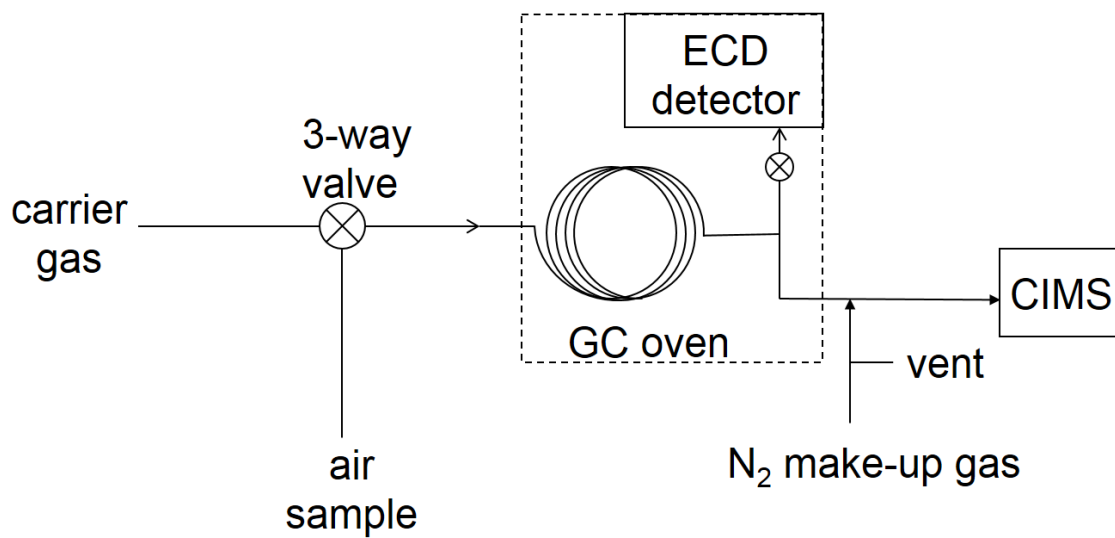
913

914 Table 2. Initial conditions for IN yield experiments.

Expt. number	Isoprene (ppb)	Isopropyl nitrite (ppb)	NO (ppb)	Expt. duration (min)
1	140	180	160	16
2	80	180	130	15
3	70	180	130	12
4	120	180	125	14
5	90	180	220	14
6	75	180	210	12
7	85	180	2400	54

915

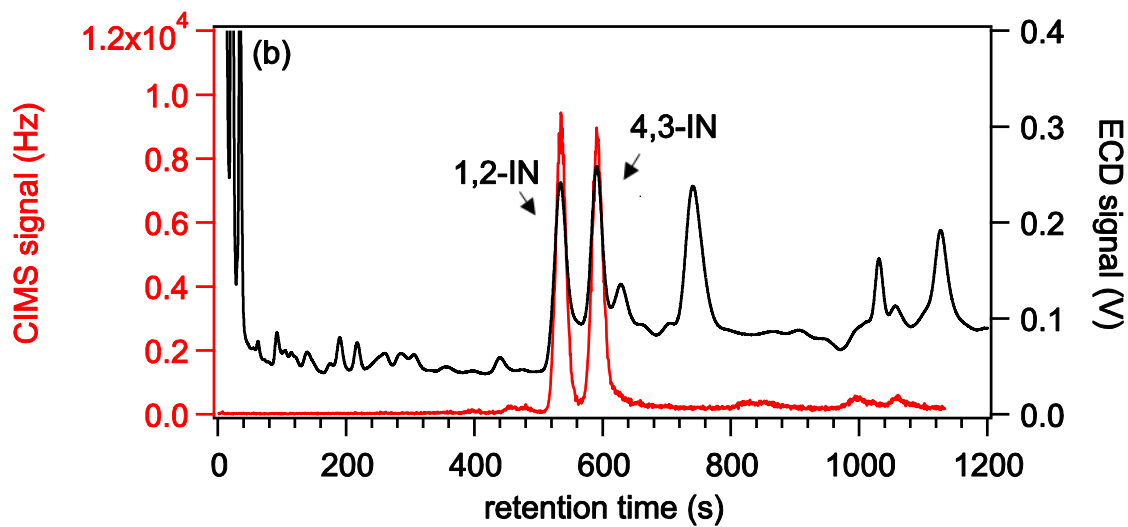
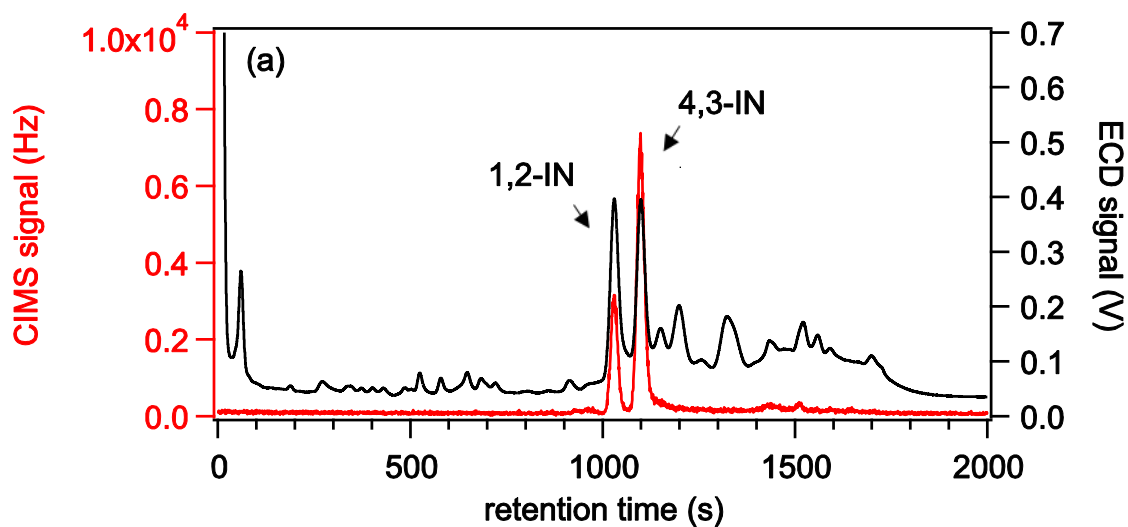
916



917

918 Figure 1. GC-ECD/CIMS setup for the CIMS sensitivity of 1,2-IN relative to 4,3-IN.

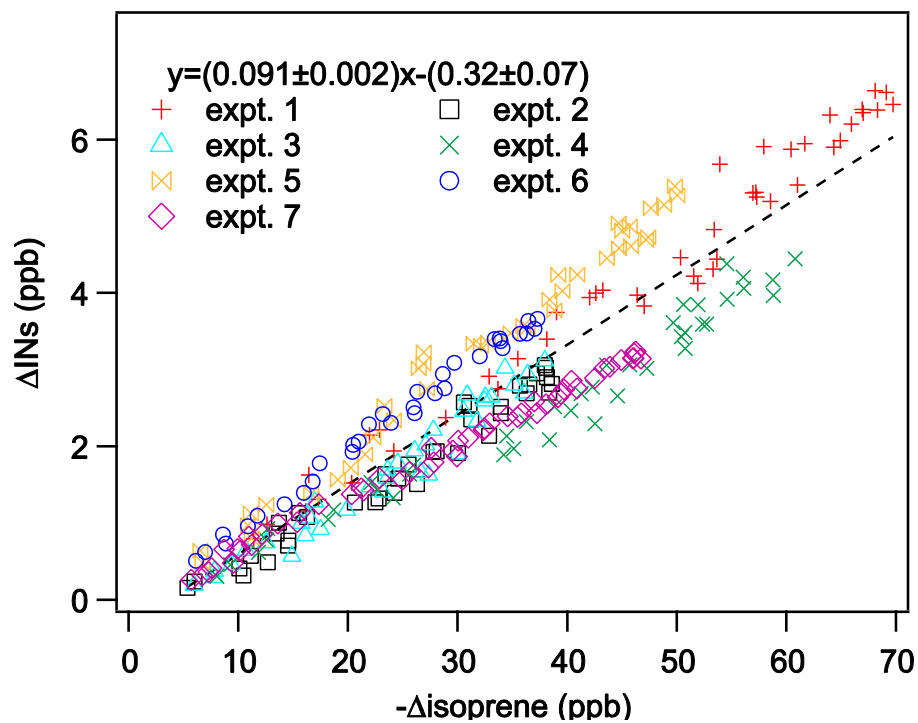
919



920

921 Figure 2. GC-ECD/CIMS chromatogram with water (a) and without water (b) added to
922 the CIMS. The ECD signal is in black and the CIMS signal is in red.

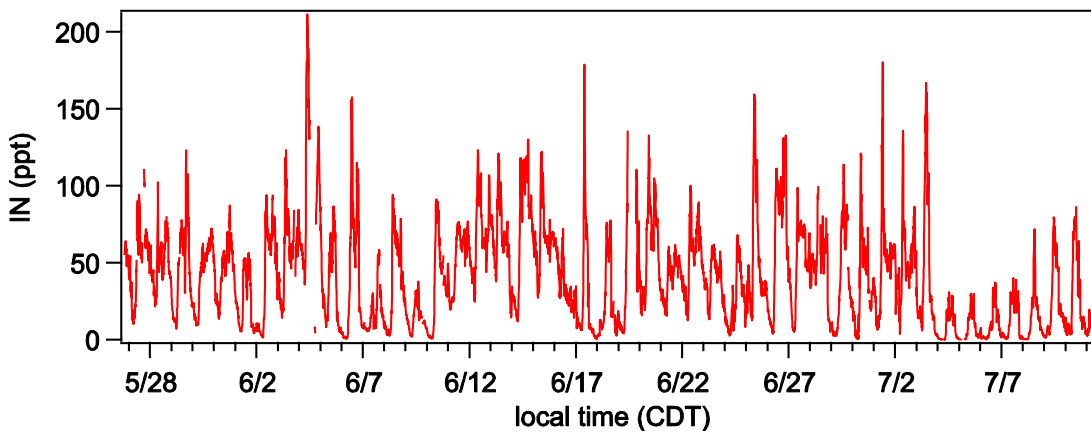
923



924

925 Figure 3. IN and isoprene data for chamber experiments. An average yield of 9% was
926 obtained from data of the seven experiments.

927

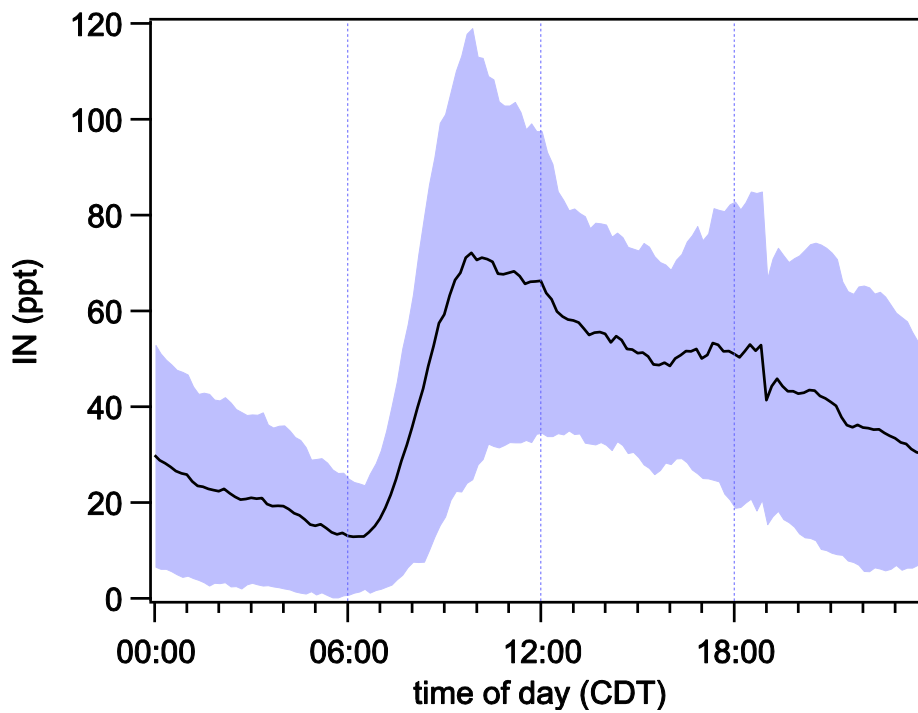


928

929 Figure 4. IN observed during SOAS.

930

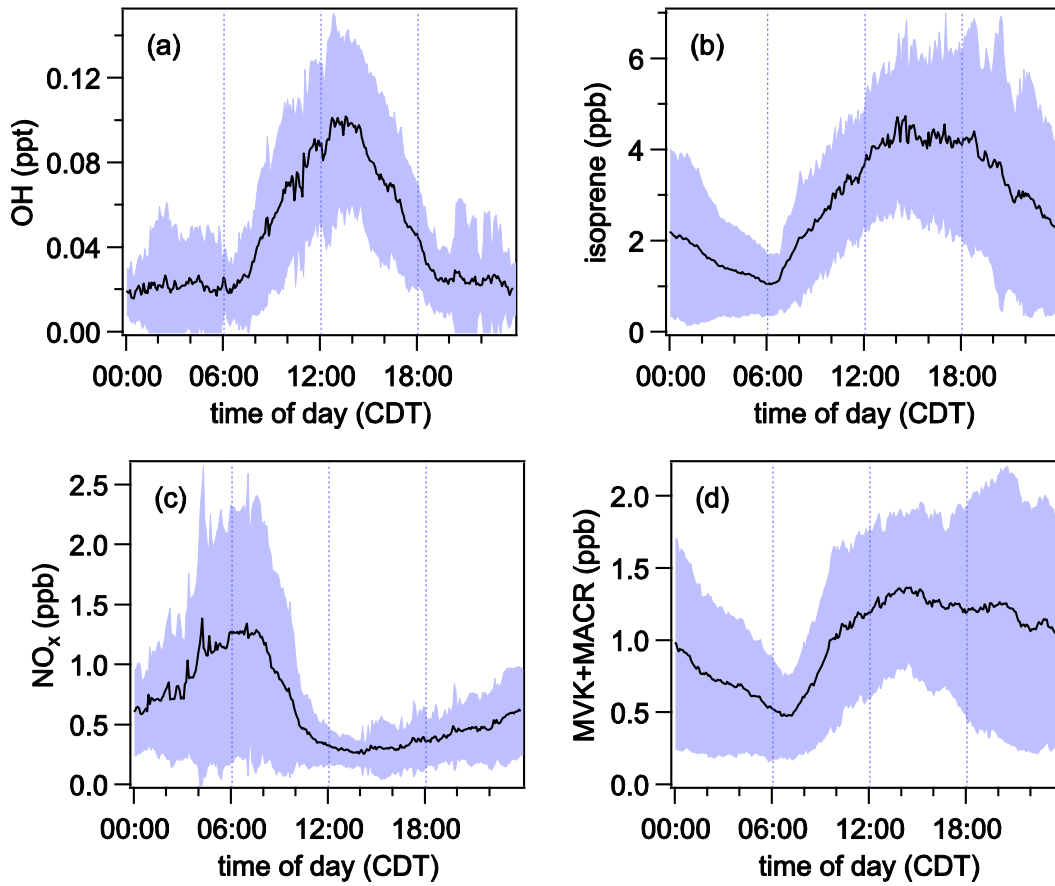
931



932

933 Figure 5. IN diurnal average from May 28 to Jul 11. The blue shade indicates day-to-day
934 variation (1σ). The abrupt drop of concentration at 7 PM is caused by instrument
935 fluctuation during its daily maintenance.

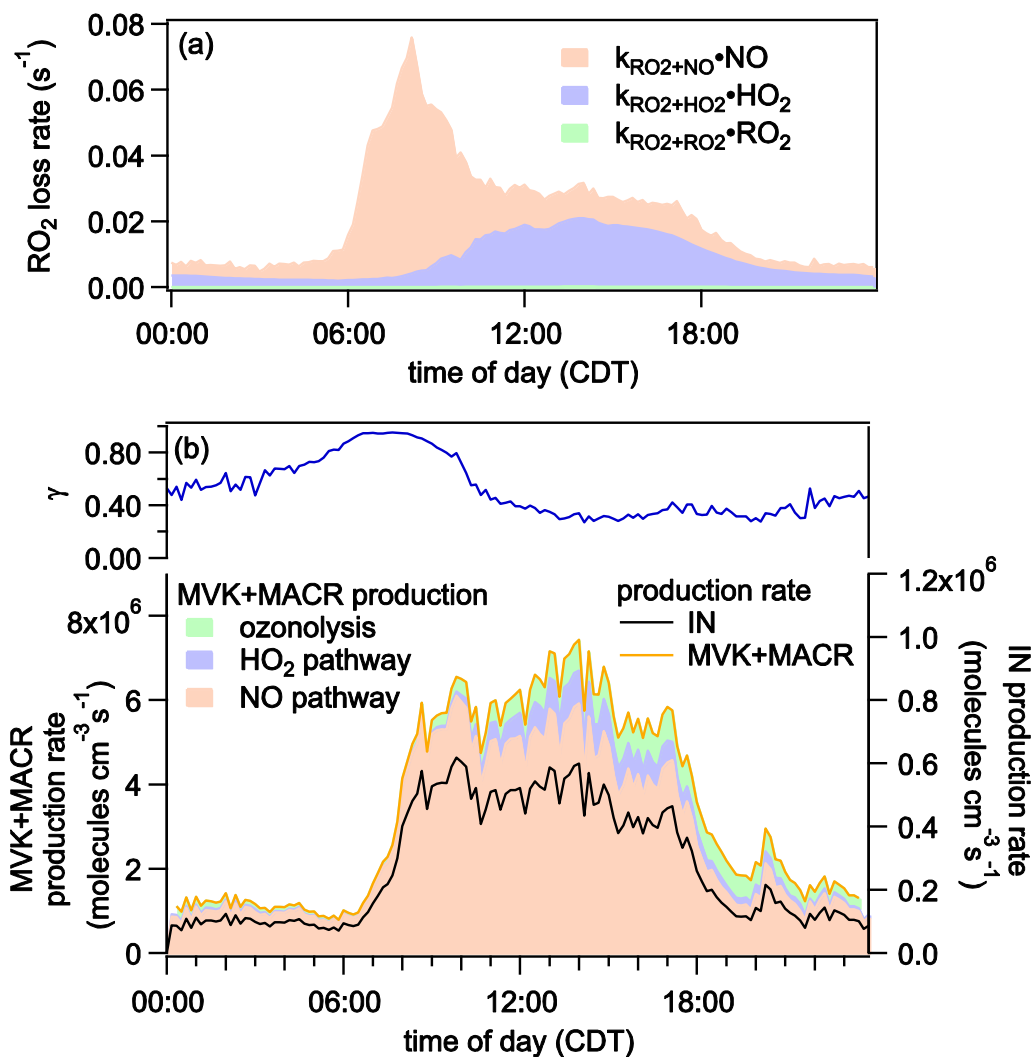
936



937

938 Figure 6. Diurnal average of OH (a, Jun 13 - Jul 3), isoprene (b, Jun 16 - Jul 11), NO_x (c,
 939 Jun 1 - Jul 15) and sum of MVK and MACR (d, Jun 16 - Jul 11).

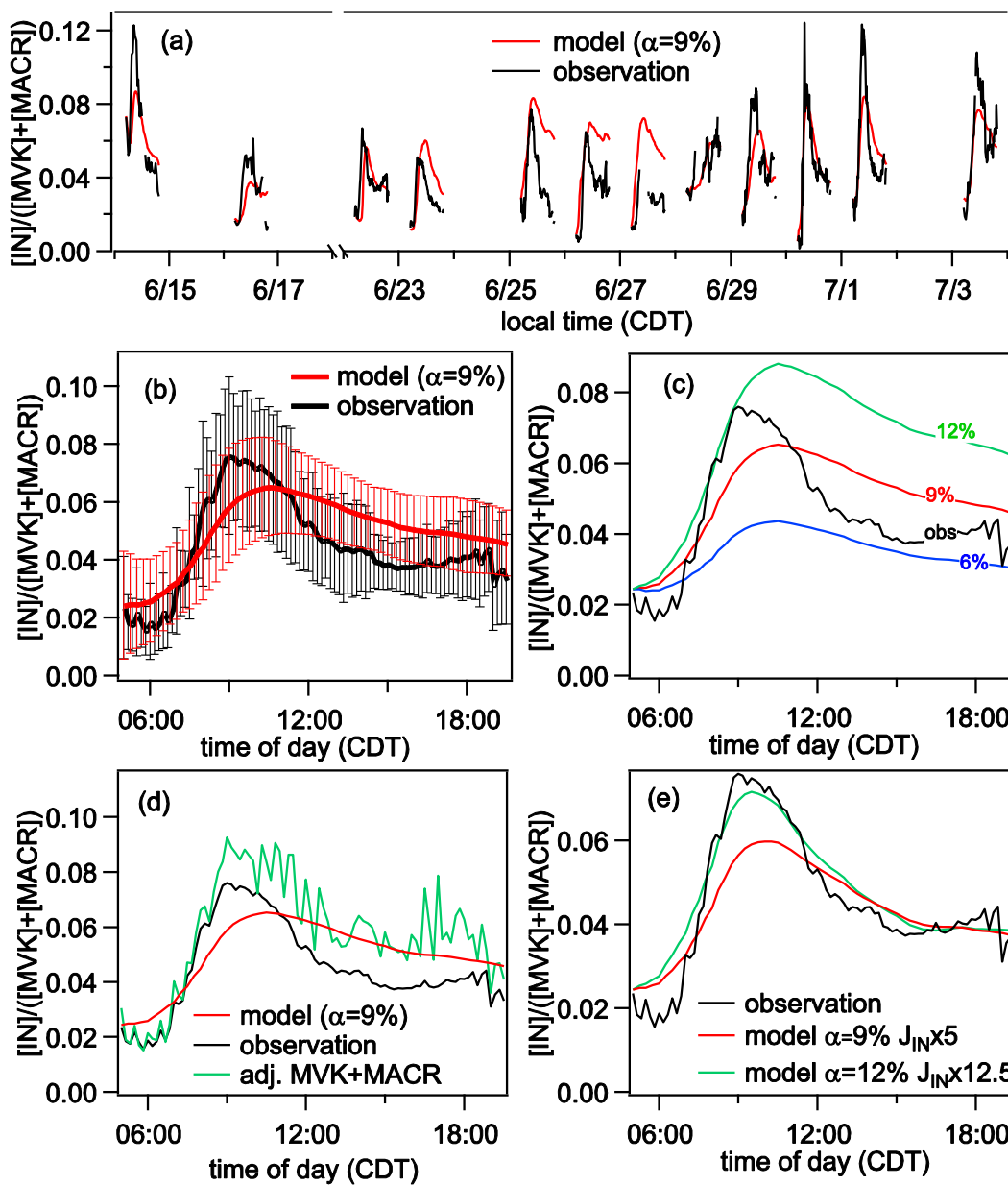
940



941

942 Figure 7. (a) Diurnal average of RO₂ loss rates for reaction with NO, HO₂ and RO₂ from
 943 Jun 22 to Jul 7. (b) Diurnal average of γ value and production rates of IN and
 944 MVK+MACR from Jun 22 to Jul 7. For MVK+MACR, production from the three
 945 reaction channels are shown in different colors.

946

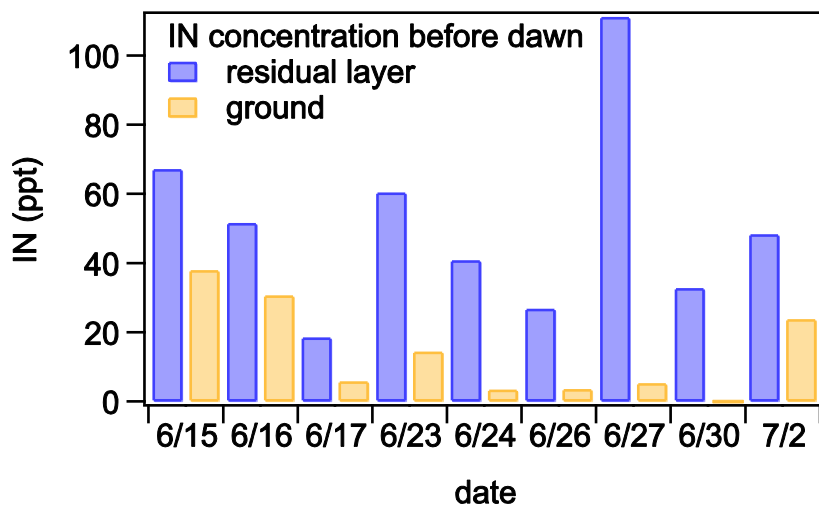


947

948 Figure 8. Simulated and observed $[IN]/([MVK]+[MACR])$ ratio. (a) Results for each
 949 selected days. (b) Averaged results over the 12 days. The error bars represent day-to-day
 950 variation. (c) Sensitivity test with IN yield set as 6%, 9% and 12% in the model. (d)
 951 MVK+MACR data was adjusted by subtracting observed IEPOX+ISOPOOH
 952 concentration from observed MVK+MACR concentration. (e) Results with enhanced IN
 953 photolysis rate.

954

955

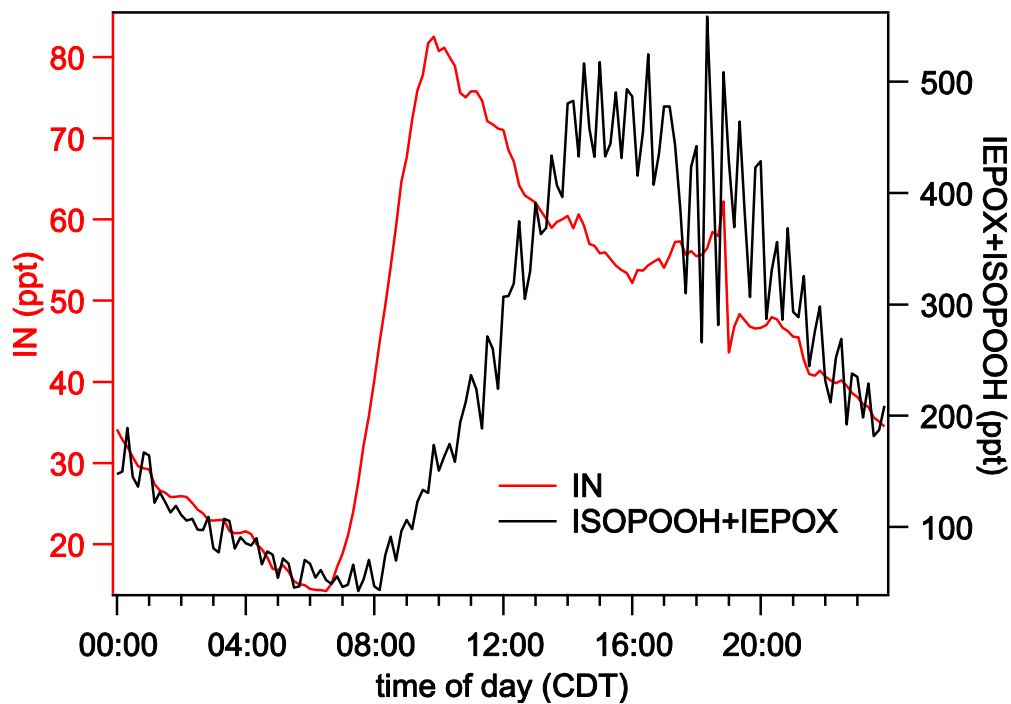


956

957

958 Figure 9 Modeled IN in the residual layer and IN observed near ground before dawn the
959 next day. The model includes IN production from isoprene oxidation by NO_3 and IN
960 consumption by reaction with OH, O_3 and NO_3 . The modeled IN may be biased, as
961 concentration change caused by transport is not considered.

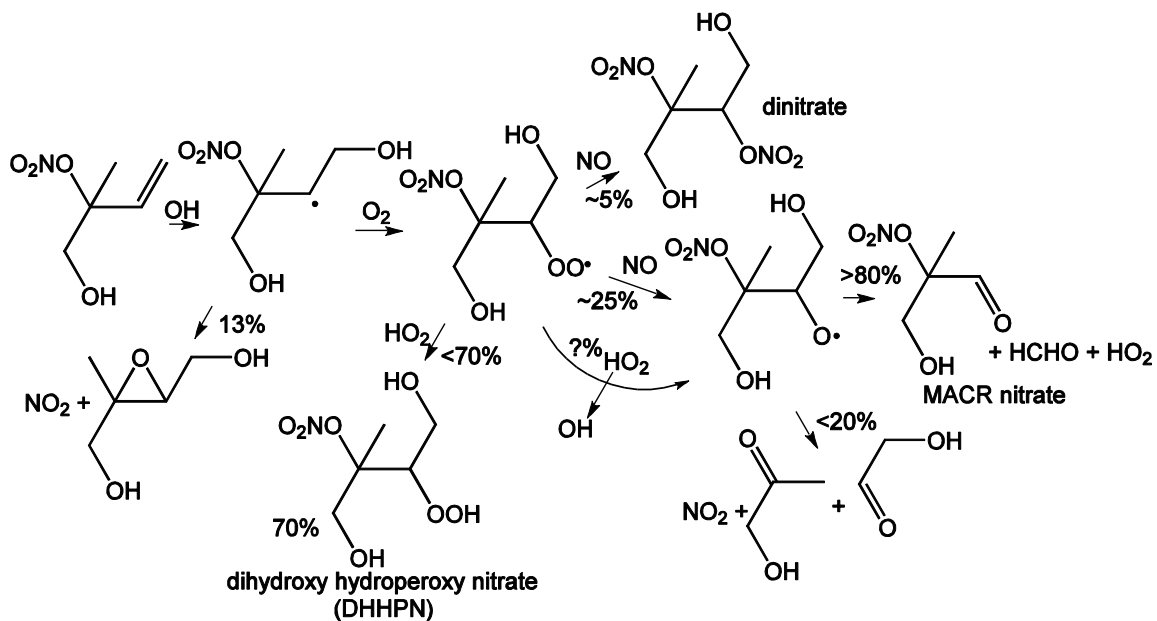
962



963

964 Figure 10 Diurnal averages of IN and ISOPOOH+IEPOX from May 30 to July 4.

965



966

967 Figure 11 Possible oxidation mechanism for 1,2-IN with $\gamma=0.3$.

968